Steels for rail axles – an overview

Article *in* Critical Reviews in Solid State and Material Sciences · April 2024

DOI: 10.1080/10408436.2022.2137462

4 authors:

Desmond Klenam
University of the Witwatersrand

Lesley Heath Chown
University of the Witwatersrand

Jones Papo
Mintek

Lesley A. Cornish
University of the Witwatersrand

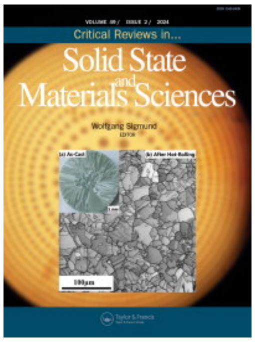

Taylor & Francis
Taylor & Francis Group

Critical Reviews in Solid State and Materials Sciences

ISSN: (Print) (Online) Journal homepage: www.tandfonline.com/journals/bsms20

Steels for rail axles - an overview

D. E. P. Klenam, L. H. Chown, M. J. Papo & L. A. Cornish

To cite this article: D. E. P. Klenam, L. H. Chown, M. J. Papo & L. A. Cornish (2024) Steels for rail axles - an overview, Critical Reviews in Solid State and Materials Sciences, 49:2, 163-193, DOI: 10.1080/10408436.2022.2137462

To link to this article: https://doi.org/10.1080/10408436.2022.2137462

Published online: 29 Oct 2022.

CRITICAL REVIEWS IN SOLID STATE AND MATERIALS SCIENCES
2024, VOL. 49, NO. 2, 163–193
https://doi.org/10.1080/10408436.2022.2137462

Steels for rail axles - an overview

D. E. P. Klenam[a,b,c], L. H. Chown[a,b], M. J. Papo[b,d], and L. A. Cornish[a,b]

[a]School of Chemical and Metallurgical Engineering, University of the Witwatersrand, WITS, Johannesburg, South Africa; [b]DSI-NRF Centre of Excellence in Strong Materials, hosted by the University of the Witwatersrand, WITS, Johannesburg, South Africa; [c]Academic Development Unit, Faculty of Engineering and the Built Environment, University of the Witwatersrand, WITS, Johannesburg, South Africa; [d]Advanced Materials Division, Mintek, Randburg, South Africa

ABSTRACT
The comparative assessments and an overview of mechanical, chemical, and physical properties of rail axles are presented. This review focused on the effects of compositions and microstructure on fatigue, fretting and corrosion fatigue of rail axles. The two main steel grades: low carbon steels for commuter trains and high strength low alloy steels for high-speed trains have ferrite-pearlite microstructures with 20–40 µm ferrite grain sizes. Minimum allowable yield and ultimate tensile strengths are 330 MPa and 600 MPa, and the minimum longitudinal and transverse toughnesses are 35 J and 22 J. Most axle failures are associated with surface and sub-surface defects with micro-cracks nucleating from ballast (small-sized pebbles in rail tracks), minute oscillatory movement leading to fretting, microstructural inclusions, and corrosion pits. The implications for structural integrity are highlighted and areas for future research directions are highlighted.

KEYWORDS
Rail axle; endurance or fatigue limits; microstructure; plain carbon and alloyed steels; mechanical properties

Table of contents

CONTACT: D. E. P. Klenam desprimus@gmail.com

1. Introduction

An effective transportation system is a fundamental pillar of developed economies. In Europe, the transport sector contributes ~10% to the economy.[1] Globally, the transport sector is intermodal and complimentary, but rail transport is by far the safest, most reliable and cheapest (Table 1).[2] Air transportation is expensive, and many cannot afford as nearly half of the world population are below the poverty line.[3] Water transport is slow and expensive – not a viable option.[2] The default is land, either by road or rail.[2] Road is cheap and widely patronized due to increased availability of vehicles. However, its challenges are bad road networks, vehicular traffic in most cosmopolitan and metropolitan cities (due to increasing urbanization in developing countries), increased global warming and environmental pollution and high vehicular accidents with associated increased deaths (Table 1).[2]

Rail transport is safe, although the mechanical components (e.g., rail axles and wheels) do fail. Rail axles are subjected to dynamic loading, with a working life of ~30 years (10^9 loading cycles).[4–6] The axles are made from medium carbon and high strength low-alloyed steels. Derailment due to rail axle failure led to the pioneering work in fatigue studies in the late 18th Century.[5–7] Many of the failures were predominantly due to poor material choice and defects due to corrosion and ballast impact. Most of these broken axles were studied, in-service stresses analyzed, and failure modes assessed, leading to standards and ways to improve structural integrity.

In the 1970s, the *Union Internationale des Chemis de Fer (UIC)* developed UIC 811-1 standards recommending the EA1N and EA4T steels for railway axles across Europe.[8–14] These carbon steels had ferrite-pearlite microstructures with yield and UTS of 330 MPa and 600 MPa. The European Committee for Standardization (CEN) then approved the EN 13103, EN 13104 and EN 13261 standards in 2008 for design conformity.[8–14] Similar standards were also reviewed in North America, Asia, and Australia, assessing shortcomings. One such shortcoming is poor corrosion resistance. Generally, rail axles were not designed for corrosion since the emphasis was on strength. Alloy steels have been developed with higher yield strength, ultimate tensile strength, toughness and corrosion resistance than the UIC 811-1 standard steels.[9,15–19]

Rail axles produced from medium carbon steels had the solid-axle configuration and were about 70% of the weight of the bogie. Coaches with these axles had speed limits below 120 km/h, partly due to the dead weight of the chassis and the high payloads, resulting more fuel consumption. The weight of solid axles is very high, 1.8–3 T, and depends on the train and the bogie system. However, high-speed bullet trains with speeds up to 350 km/h use a hollow axle configuration, which are produced from high strength low-alloy (HSLA) steels with strengths above 800 MPa and give about 20% weight reduction. The HSLA steels have better mechanical and corrosion resistance, making them better than medium carbon steels.[9,15–19]

Typical alloying elements in the HSLA steels are Cr, Ni, Mo, and V, together with P, Si, Cu and S contents of standard steels. HSLA steels have strong carbide formers, such as Cr, V and Mo, which lower the cementite (Fe_3C) proportions, since they form different carbides from iron carbide, thereby reducing the amount of free C available for Fe to form Fe_3C. Recent reviews focused on rail axle design concepts, mechanical fatigue and periodic inspections on structural integrity.[6,20–26] However, an appraisal of country-specific standards and variation in compositions of rail axle steels has not been done and is needed because of the effect of composition variation on corrosion and mechanical properties. Thus, the purpose of this review is to provide comparative assessment of rail axle steel grades highlighting the composition-structure-property relationship and its effect on structural integrity of typical commuter and high-speed train axles. An overview of fatigue, corrosion-fatigue, and fretting fatigue failure mechanisms, which are main failure modes of rail axles are also reviewed considering recent developments made to mitigate against them. Rail axle steels grades from Europe, Asia, North America, Australia, and Africa were grouped into two classes based on their phase proportions. The paper concludes by identifying future research directions.

Table 1. Fatality risk of passengers using different mode of transport in the European Union from 2008–2010.[2]

Mode of transport	Fatalities per billion passenger kilometers
Airline passenger	0.1
Railway	0.16
Car occupant	4.45
Bus/coaches	0.43
Powered two-wheeler	52.59

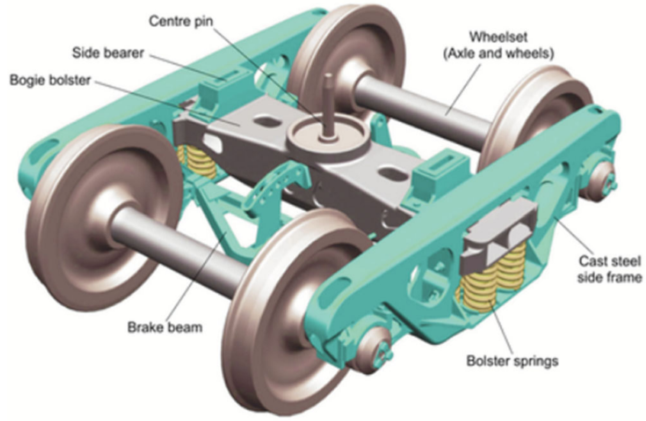

Figure 1. Typical bogie system of a freight car.[27,28]

2. Overview of railway axles

2.1. Rail bogie – an overview

A typical rail bogie system is shown in Figure 1 with key components being a bogie frame, suspension system and axle box suspension.[27,28] The bogies experience high stresses as they carry the dead-weight and payloads of the train. About 70% of the weight of the bogie is the rail axle.[15,25,29–32] A coiled spring and axle box suspension absorbs shocks between axle bearings and bogie frame. The axle box suspension is placed between the axle bearings and bogie frame to ensure vertical and not lateral movements.[31] The wheelset comprises bearings, wheels, axle box, brake disk, gear system and axles,[6,24,30,31,33] and is a pressed fit of the assemblage of the wheels and axle, which is held together by friction.[34,35]

Rail axle bearings allow rotary motion and are subjected to impact loads from rail joint, switches, wheel flats, static and dynamic loads.[36–39] They also experience axial loads resulting from lateral movement of trains on curved rails or snaking motion.[40,41] Roller bearings are used to reduce frictional torques, increase operating speed, and can accommodate temperatures as high as 200 °C of the bearing casings to prevent "hot box" failure (overheating of the roller bearing due to increased friction).[40,41]

2.2. Rail axles – an overview

Rail axles transmit driving torque to the rail wheels and maintain the positions of the wheels relative to each other and the chassis of the train.[7,19,42] Any damage to the rail axle can result in derailment, which can be catastrophic.[7] Thus, safety measures and design protocols ensure continual performance in service. Periodic inspections based on the damage tolerance principle are used for early crack detection to prevent cracks reaching critical sizes.[7] Rail axles are classified as freight wagon axles, coach axles and locomotive axles.

In 2011, the European Railway Agency (ERA) reported 329 railway axles broken between 2006 and 2009.[43] Most of these failures were attributed to fatigue due to the cyclic nature of the applied stresses.[5,19,26,44,45] Figure 2 shows the areas susceptible to fatigue, which includes all press-fits (wheel seat, brake disk seat, bearing seat and labyrinth seal seat (areas labeled 1 on Figure 2)) and the axle fillet radii (point 2 on Figure 2).[46] Notches and transitions around the plain parts of the axle are prone to fatigue failures.[19]

The ratio of the diameter of pressed fitted part (D) to the journal (d), affects the fatigue strength of the railway axles (Figure 3).[19] For smaller D/d ratios (~1.0), the pressed fitted parts are susceptible to crack nucleation. Cracks nucleate beneath the press fits by fretting.[19,42] As the D/d ratios increase, fatigue failures occur in the mid-span section of the axle and the fillets become critical regions for crack nucleation.[47] For typical Shinkansen axles used in Japan, the pressed fitted parts are more susceptible to crack nucleation due to the smaller D/d ratios (~1.10) compared to much higher values for other standards (~1.15), Table 2.[5,48] Thus, typical European axle journals are the areas prone to crack nucleation due to high D/d ratios.[5,48] Based on the D/d criterion, axles produced in Europe have good fatigue strength at the press-fitted parts, whereas there is good fatigue strength in the journal for axles produced in Japan.[47] Axles for high-speed trains in Europe are annealed, while the Shinkansen axles from Japan are induction-hardened for increased surface hardness, wear resistance, and longer fatigue life from a hardened outer layer around the tougher inner core.[49] Induction-hardening for the Shinkansen axles induces high compressive residual stresses to a

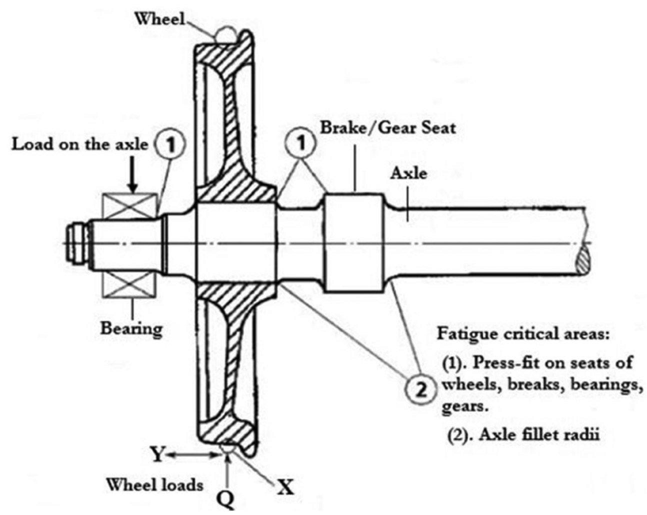

Figure 2. Rail axle regions susceptible to fatigue failure.[46]

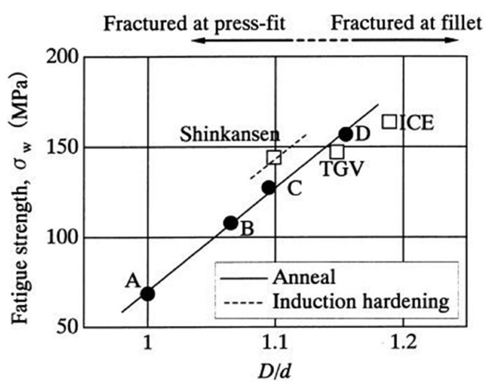

Figure 3. Effect of diameter ratio of press fitted parts to the journal on the fatigue strength of rail axles in Japan and Europe.[20]

Table 2. Fillet radii and diameter ratios of high-speed trains.[47]

Measurement	Shinkansen (Japan)	TGV (France)	ICE (Germany)
Diameter (D)	209	212	190
Diameter (d)	190	184	160
D/d	1.10	1.15	1.19
Radius (mm)	100	15 & 75	15 & 75

depth of 10 mm, allowing higher stresses (up to 147 MPa) than the 80 MPa for European axles.[50] The effect of the final processing on fatigue strength is shown in Figure 3.[47] Other processes to induce beneficial residual stresses include forging, rolling and the differential shrinking and cooling (quenching stresses) at the surface and core of railway axles during secondary heat treatment processes.[51]

The structural durability of railway axles depends on fatigue strength and the service stresses.[26,42,46] This is largely influenced by the material properties, design, manufacturing and environmental factors, such as localized atmospheric corrosion and ballast impacts.[42]

To benchmark the fatigue strength of railway axle materials, testing is done under constant amplitude stresses for 10^6 - 10^7 cycles, which is below the endurance limit where no fatigue failure is expected,[26,46] to determine the endurance limit. In service, the cumulative effect of stresses (constant and/or fluctuating) on the railway axle can cause premature failure by exceeding the predicted loads.

Corrosion,[15,46,52,53] fretting at the press-fits [48,52,54] and ballast impact [6,46,53,55] causes dents, micro-voids, scratches and gouges on the axles, providing stress raisers which can initiate cracks that could lead to catastrophic failures at stresses below the fatigue limit of the axle once these cracks exceed their critical sizes.[15,46,52] A surface dent of 3 mm could increase localized stress by at least 3%, which reduces the endurance or fatigue limit of the axle.[15] The Rail Sciences Laboratory [15] identified the cause of premature axle failure, especially below the predicted endurance limit, as either surface damage or journal fretting.

2.3. Overview of design approaches of railway axles

Although railway axles are designed for a ~30 year life, they sometimes fail in service prematurely,[6,9] so a combination of safe life design and routine inspections based on damage tolerance principles is used.[6] Standard design of axles is the 'safe-life' approach, where stresses induced on the axle are kept lower than the fatigue limit (endurance limit), to prevent premature in-service failures. In Europe, EN 13103 standard was designed for non-powered (trailing) axles,[8] and EN 13104 governed powered (driving) axle designs.[8] There are also Japanese [18,22] and North American [17] standards.

Limitations in current design methods for rail components and standards have been criticized.[6,26] For example, maximum allowable loads are estimated based on constant amplitude loads, which may be suitable for worst-case scenarios and maximum allowable stresses. However, these estimates do not adequately cater for in service dynamic amplitude loads (payloads), variation in track quality, mechanical and surface damage such as corrosion, fretting and ballast impacts.[6,9] Railway axles are exposed to high number of loading cycles, ~10,[9] which exceed the endurance limits of axle steels, 10^6 - 10^7 cycles, and premature failures have occurred.[20–23]

Periodic inspection and maintenance protocols are used to ensure structural integrity. In Europe, the EN 13103 and 13104 standards specify the durability validation criteria for railway axles.[8] Fail-safe and damage tolerance principles are used to improve working lives of axles and structural components.[6,29,30] Fail-safe is characterized by redundant design and designing for crack arrest (so the cracks do not grow). Micro-cracks at the surface/sub-surface are detected before they reach critical defect sizes in damage tolerance, by periodic inspections.[30,56] The inspection intervals are determined using the probability of detection (PoD) approach.[24,57,58] Nondestructive techniques, such as ultrasonic testing, magnetic particle inspection and eddy currents, are used for determination of cracks in axles in service.[6,20–26] Damage tolerance is also used to correlate crack depth and the number of loading cycles.[6,24,25,59] Modifications in design approaches for rail components, especially axles and wheels, were proposed.[5,20–23,59]

2.4. Effect of service stresses on railway axles

Stresses on railway axles could be static, dynamic, torsional (due to braking and traction, press-fit loading), residual (induced by manufacturing process e.g., heat treatment, forging, rolling), higher frequency loading (stick-slip behavior), bending and axial tensile (stresses at crossovers, curved sections of tracks and switches on rail lines). The impact of these and the possible failures and accidents caused has been investigated and documented.[20,25,41,48,60–62]

Axial compressive and tensile loads are generated beneath the press seat and the fillets, which affect the mean stresses, the stress ratios and hence the fatigue strength of the axles. Micro-slip at the contacting surfaces of the axle and the wheels could be sites for crack nucleation. Defects from the asperities (surface roughness) of the contacting surfaces (axle-wheel interface) could result in slip displacement causing shear stresses and these can nucleate micro-cracks on the surface of the axle, which lower fatigue strength, and could lead to premature failure of the axle, if the micro-cracks were not detected early. Multiple crack nucleation and the cumulative effects of shear stresses give high scatter in the stress - number of cycles to failure (S-N) data. For HSLA steel grade 34CrNiMo6, reduced fatigue limit under rotating bending occurs in the press fitted regions.[48] Significant reduction in fatigue strength is attributed to fretting fatigue at the press fits.[26]

During braking and traction, the effect of torsional stresses induced within the axles is detrimental. Although torsional stresses are negligible compared to other stresses acting on the axles, their cumulative effect can be detrimental as they can nucleate micro-cracks on the surface and sub-surface of the axles. The magnitude of torsional shear stresses varied depending on weather conditions,[61] especially wet and dry.

At curved track sections, crossovers and rail line switches, stresses are induced in the rail axles. At curved sections, most of the load is transferred unto the outer wheel becoming bending stresses in the axle with the disk of the wheel acting as the lever arm. There is direct correlation between the bending moment of the axle and the wheelsets: the outer wheels contribute to the maximum bending stresses experienced by the axle. A slight change in alignment can contribute to the axle failure and increased axle loading occurs in small-radius curves during curving of tilting trains.[61]

The dynamic and static loads induced in axles can result in failure. The weight of the chassis of passenger or freight trains induces bending stresses on the axles between the wheels. In service, the bending stresses are increased significantly by the cumulative effect of the dead weight (structural weight of the train) and the increased payload (weight of cargo in freight trains or weight of passengers with its associated loads in commuter trains) conveyed. The impact of the dynamic and static loads result in irregularities such as out-of-round wheels which increase bending stresses on the axle by 20%.[61]

High frequency loading can lead to stick-slip and out-of-phase oscillations of the wheelsets and the rails.[62] Stick-slip is a friction phenomenon, caused by vibration of the wheels and rails [63,64] and occurs in dynamic systems where friction is attributed to the velocity difference of the two contacting surfaces in sliding motion. The kinetic energy due to the relative motion of the contacting surfaces dissipates by forming microscopic particles or asperities, which become debris that can cause micro-cracks between the surface of the axle and wheel. It occurs by both elastic deformation of the asperities of the contacting surfaces when sticking together, and plastic deformation of the contacting surface during the sliding motion. In high-speed trains, the loading frequency from the wheel rotation does not exceed 30 Hz, thus not allowing sufficient vibrations in the wheel-rail interactions to cause fatigue.[65] High frequency oscillations in wheel-rail interactions cause bending stresses in the rail axles,[61] and increase torsional moments in the axles during driving and sudden braking of the train. Torsional shear stresses increased from 7 MPa to ~100 MPa in extreme stick-slip cases,[62] initiating cracks at the axle surfaces, which if not detected early, could lead to complete rupture.[62] Stick-slip produces the squeaking sound when a train is stopped.

Residual stresses are process-induced stresses, and occur without external stresses [48]. The effect of residual stresses on a component is similar to externally applied stresses, and could lead to distortion and warpage in mechanical components when service stresses are applied, which could affect structural integrity.[66] Residual stresses can be beneficial (compressive) or detrimental (tensile), by raising or lowering the mean stress experienced over a fatigue cycle.[67] The manufacturing processes of railway axles induce residual stresses and can influence the fatigue strength, breaking strength, and corrosion resistance. Tensile residual stresses can nucleate micro-cracks during fatigue, so having compressive stresses at the surfaces helps prevent this. Techniques used to promote compressive stress include shot peening, laser peening, autofrettage, cold hold expansion and case hardening.[67] Surface defects (which could initiate crack nucleation and lead to premature failure at low applied stresses) are inhibited by in-plane compression, due to compressive residual stresses at the surface. When a surface is in compression, the core experiences counterbalancing tensile stresses, making it defect-free with sufficient inherent strength to prevent failure.[67] Undesirable tensile residual stresses tend to nucleate new cracks and/or propagate existing cracks, which could lead to premature failure. The origin of residual stresses includes inelastic or plastic deformation, temperature gradients during thermal cycles and microstructural changes or phase transformations.

Relieving residual stresses is achieved by normalizing with controlled cooling, resulting in finer microstructures in axles produced from EA1N steel.[8,9] For axles produced from quenched and tempered EA4T steel, the residual stresses are induced from rapid cooling (quenching stresses) of the hardening processes. Tempering between 260 °C and 760 °C has negligible effect on relieving residual stresses. Final machining and cold working can also relieve detrimental tensile residual stresses.

3. Overview of failure mechanisms in railway axles

Most axle failures are either environmentally induced or due to operating conditions which induce stresses that could lead to catastrophic damage. Most failures and derailment resulted in much property damage and life loss.[68,69] Resistance from the wind (drag force) is a load and the cumulative load effects can contribute to rail derailment. Wear and corrosion also increase stresses, resulting in railway axle failures. Other load effects due to operating circumstances include train misalignment.[54,70] The two main failures of railway axles [41] are from overheating of the bearing and fatigue.[19]

3.1. Failure by over-heating of roller bearings

Roller bearings are made from copper alloys, and failure by over-heated roller bearings (‘hot box’) is from increased friction in the bearing, due to irregularities,[41] copper penetration from the roller bearings into the grain boundaries of the railway axle steel at high temperatures, or inadequate lubrication of the parts in contact. When regions around the axle and the locking ring of the bearing box are stressed at high temperatures, copper precipitates at the steel’s grain boundaries, causing embrittlement, promoting sub-surface cracks, damaging the structural integrity of the axle.[71] Excessive heating of the bearing results in complete failure of the axle, known as “burnt-off journal” (Figure 4).[41,72]

3.2. Failure by fatigue

Fatigue is predominant in railway axle failures, and rail axles were among the first mechanical components identified to have failed from fatigue.[73] Fatigue is a surface and sub-surface-related mechanism, resulting in a progressive localized permanent structural damage in components subjected to conditions of

Figure 4. Rail axle failure due to over-heating of the roller bearing.[41,72]

fluctuating, repeating or alternating stresses locally, which culminates in micro-cracks and finally complete rupture after the fatigue life of the component is exceeded.[73,74] The acceptable mechanism of fatigue in ductile materials is effect of cyclic plasticity involving the movement of dislocations which results in alternate blunting and resharpening of any preexisting crack tip while advancing.[75–78]

The fatigue life 'N_f' is the number of cyclic loads a component can sustain before it ruptures. The S-N or Wohler curves, which are plots of the stresses to the number of cycles to failure, are used to determine the fatigue strength of a material.

Potential mechanisms causing surface defects (Figure 5) at the wheel seat, axle shaft and transitions include fretting fatigue dimples,[52,80–83] hard nonmetallic inclusions at or beneath the surface of the axle,[23,38,54,84–86] local ballast impacts indenting the wheel seat or axle surface,[24,50,80,87] corrosion pits/corrosion fatigue, turning marks (grooves, offsets) ,[23,38,54,84–86] stress concentrators and surface asperities,[23,38,52,54,80–86] which increase the surface roughness of the axle or wheel seats. If not detected and remedied, these can result in fatigue failures in the presence of increased fluctuating stresses. Axle fatigue failures have flat and smooth cylindrical surfaces, with or without shear lips, and characteristic beach marks. The areas of the axles susceptible to fatigue are shown in Figure 6.

Failure by fatigue occurs in three main stages. Stage 1 is associated with crack initiation and is promoted by defects such as pits, precipitates, and inclusions. These are mainly sub-surface and or surface defects which create geometrical discontinuities. Typical nucleated cracks on rail axles have depths of at least 250 μm. Most of these cracks are parallel and at ~60° to the contact surfaces (Figure 7a). The crack initiation paths are determined by the ferrite-pearlite morphologies and inclusions. Stage 2 is where cracks start propagating while new cracks nucleate, making it a continuous process. During this stage, initially some of the cracks propagate between the pearlite lamellae (Figure 7b), and later the same cracks can be independent of any microstructural feature (Figure 7b and pass transversally through the pearlite lamellae. Stage 2 is characterized by striations, due to the fluctuating load and hence incremental growth of the fatigue cracks. Once the cracks exceed the critical size, the final stage is reached, where the component fractures in a brittle manner as the residual area is too small to support the applied load on the structure.

For rail axles, most surface defects cause decreased fatigue resistance,[88–95] because they are potential sites for crack initiation as they are stress concentration points. Thus, fatigue behavior of rail axles is controlled by the nature of surface and sub-surface cracks: thus depth, width and orientation.[96] Increased defect size and depths greatly decrease the fatigue limit and fatigue life of rail axles.[97] Material defects include: nonmetallic inclusions, minute precipitates, micro-shrinkage, corrosion pits and pores, geometric defects: minute notches from manufacturing, surface roughness and scratches.[85,98] The latter defects can cause abrupt changes in the geometry of the component, which induce high stress concentrations at these defects.[96,99,100] Regions around the stress concentration points can nucleate new cracks, while there is continuous propagation of existing cracks.[98] Typical sites for crack nucleation from ballast impacts is shown in Figure 8. The relationship between N_i, stress concentration factor, K_t and defects is described in Equation 1.[96]

$$\xi = \left[K_t \boldsymbol{\Delta}\sigma\left(1 - \frac{r^*}{\rho}\right) - \boldsymbol{\Delta}\sigma_e\right] N_i^{\alpha} \tag{1}$$

(1)where: ξ = coefficient of fatigue life; K_t = stress concentration point; $\Delta\sigma$ = stress range; r^* = distance ahead of main defect causing the crack initiation; ρ = curvature radius of the crack tip; $\Delta\sigma_e$ = fatigue limit; N_i = fatigue crack initiation cycles and α = exponent of fatigue life.

3.2.1. Corrosion fatigue and stress corrosion fatigue of rail axles – overview

Corrosion fatigue is the progressive degradation of usually uncoated rail axles or damaged areas of coated rail axles due to the cumulative effect of cyclic stresses in an aggressive environment.[79,97,101,102] The aggressive environments include atmospheric conditions such as fog, rainwater, marine and effluent

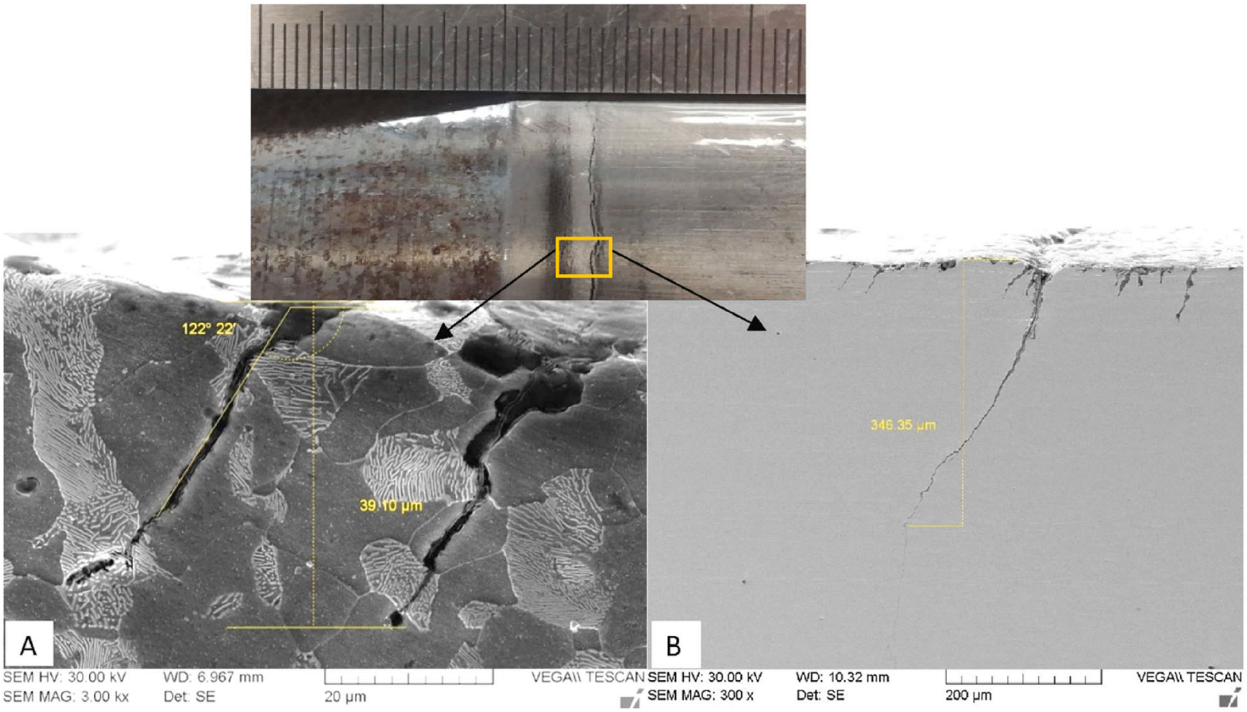

Figure 5. Multiple cracks from different nucleation sites and corroded surface at the axle seat edge.[79]

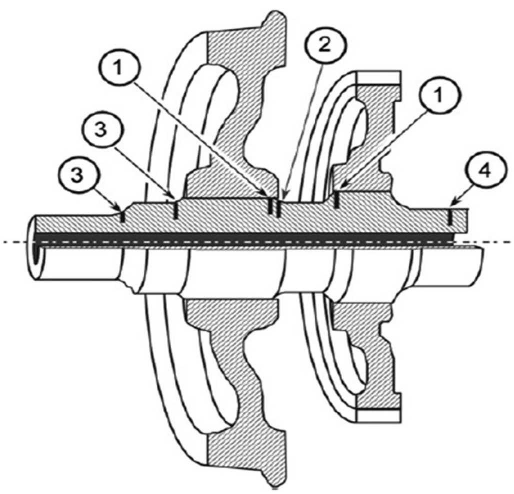

Figure 6. Sites on rail axle susceptible to fatigue failure: (1) press fit cracks beneath the wheel and gears, (2) crack at T notch transition (3) cracks at U and/or V notch transition and (4) cracks initiated largely by corrosion pits at the shaft.[6]

contamination in heavy industrialized areas,[70,103,104] which allow electrochemical reactions and are a major cause of fatigue failure in railway axles. Thus, corrosion fatigue is the interaction of irreversible cyclic plastic deformation and localized electrochemical reactions, a precursor for continuous nucleation and acceleration of minute cracks.[97,101,103] Corrosion pits and localized or general corrosion on the axle surfaces are major causes of failures.[89,97,104] The reactions of the axle to corrosive media create surface defects such as micro-cracks, scratches, pits and discontinuities at the sub-surface (often aided by stress concentration points) which propagate under cyclic loads, leading to brittle failure, if not detected early.[54,58,70,89,104] An example of combined effect of corrosion and fatigue damage at the axle seat surface is shown in Figure 9.[79] The pressing of the wheels onto the axle caused scratches (shown by arrows) which acted as corrosion initiation sites and later intensified to crevice corrosion (Figure 9b). Generally, the corrosion occurs due to the semi-enclosed gap (crevice) between the axle and the wheels, where the conditions are different. The semi-enclosed gaps are also sites for the initiation of fatigue cracks as shown in Figure 6. High corrosion rates were observed at the pressed surface due to localized pits and at the edge of the wheel seat, resulting from crevice corrosion from the semi-enclosed gaps. In the harsh environments where most trains are used, corrosion is exacerbated by the synergy between mechanical (fretting, wear and fatigue) and electrochemical actions (pitting and crevice corrosion).[79] Thus, damage due to corrosion increases the fatigue crack nucleation rates and the coalescence of these minute cracks can occur due to the corrosive action and the mechanical movement.

Fatigue failure is increased due to the corrosion providing surface defects that cause failure to take place at lower stresses and after lower numbers of cycles (N), i.e. below the fatigue limit of the railway axle material.[89,104] Corrosion products concentrate

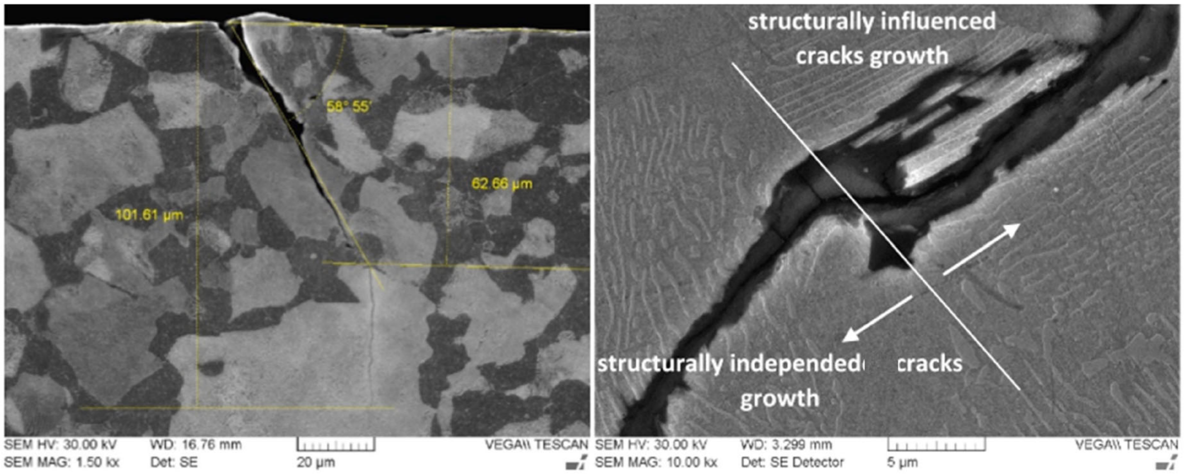

Figure 7. SEM images showing fatigue crack propagation between the pearlite lamellae initially, and some after the crack propagates transversally across the pearlite lamellae.[79]

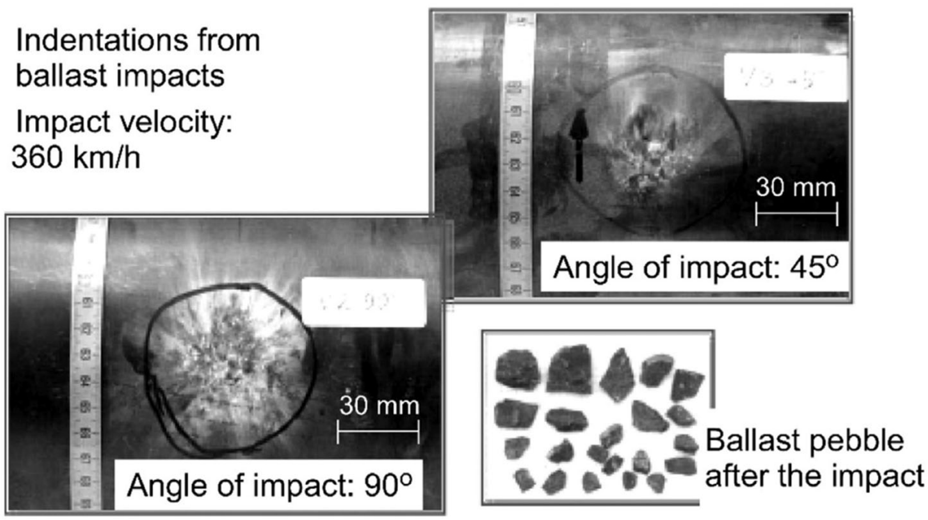

Figure 8. Crack initiation sites on typical rail axle due to ballast impact.[98]

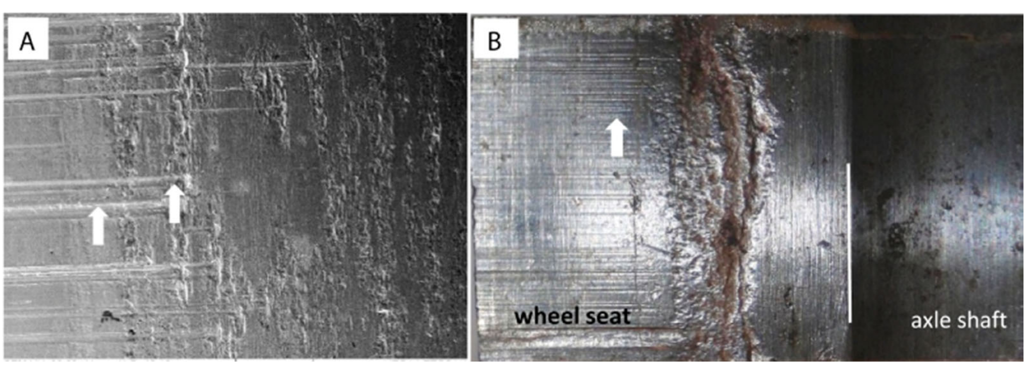

Figure 9. Initial corrosion damage (a) and intensive crevice corrosion (b) of the press-fit of the axle and the wheel seat.[79]

around the micro-notches, concentrating stresses at the notch pit.[103] This shifts the electrochemical potential to lower values, increasing the dissolution of the rail axle steel and causing micro-notch growth. As the local stresses on the axle increase, the fatigue strength decreases due to the corrosion pits. As the number of cycles increases, the cracks grow, culminating in axle failure when the cracks exceed the critical length.[104] Aside corrosion pits, minute microstructural features, e.g., inclusions and precipitates have been used to predict the fatigue strength of rail axles which agrees with experimental data.[20,48,56,79]

Table 3. Summary of failures of rail axles.

Place of failure	Causes of failure
Rickerscote, Stafford (1996)	Corrosion pits[5]
Shields Junction, Scotland (1998)	Stress corrosion fatigue[104]
Trudel, Quebec, Canada (2001)	Pitting corrosion[45]
Bennerley Junction, Nottingham (2002)	Corrosion pits[104]
Luton Station (2002)	Electric arcing[104]
Basingstoke (2002)	Electric arcing[104]
Simplon tunnel, Switzerland (2006)	Corrosion pits[109]
New South Wales, Australia (2006)	Ballast impact[110]
S Bahn failure in Germany (2006)	Fretting Corrosion at press fits[68,111]
Tichborne, Ontario, Canada (2007)	Corrosion pits[108]
Cologne, Germany (2008)	Stress corrosion cracking/Ballast impact[68]
Viareggio, Tuscany, Italy (2009)	Corrosion pits at U-Transition
Benevento Station, Italy (2019)	Fatigue at press fits[112]

High cyclic stresses of the journal and corrosive liquids on the surface of the axle could lead to stress corrosion cracking (SCC), which has a similar mechanism to corrosion fatigue, leading to railway axle failure.[103] Reviews on various aspects of SCC are available,[103,105,106] and the SCC mechanisms have been summarized.[106] Failure by stress corrosion cracking is from brittle cracking at fairly low stresses.[54] Derailments due to railway axle failure by corrosion and stress corrosion cracking in the United Kingdom,[5,15,70,104] Canada,[45,107,108] United States [15] and Europe [15,70,104] have been studied (Table 3). In North America, 52 failures of axles were documented between 1998 and 2002, most being attributed to either corrosion fatigue or stress corrosion cracking.[15] Thus, corrosion resistance of railway axles is important, and could reduce failures in rail transportation.[54]

3.2.1.1. Effect of corrosive environment on fatigue strength. In corrosive environments, crack propagation and pit-to-crack growth rates are faster than in air.[101,103] The combined effects of fatigue and corrosion result in no fatigue limit as it is suppressed with the disappearance of the "knee" in the S-N curve (Figure 10).[54,89,97,101,103] At high stress levels above the air fatigue limit of the rail axle steel, the S-N curves and the fatigue limit in air and corrosive medium are comparable.[54] Below the air fatigue limit and at relatively low stress levels, the fatigue strengths of the steel in the corrosive medium were very low. After fatigue experiments, the samples showed cracks of varying sizes around ~1 mm (Figure 10).[54]

The stress amplitude design limit for axles based on European Standard EN 13103/13014 is ~332 MPa and that of Germany, BASS is ~220 MPa.[8] The fatigue limit was reduced by at least 50% due to the effect of rain water,[54,101] than in air.[58] Similar results were also observed for AISI 1018 steel with ~120 MPa fatigue strength at 2×10^6 cycles in air, which further reduced to ~90 MPa in tap water at ~10^7 cycles.[93] When there was insufficient stress for the nucleation and propagation of cracks, especially in air, the presence of a corrosive medium promotes the initiation and propagation of cracks from the geometrical discontinuities or defects associated with corrosion.[95] These minute cracks, resulting mostly from corrosion pits, then grow, leading to total failure, i.e. decreasing overall fatigue strength.[58,107,108,113]

3.2.1.2. Pit-to-crack nucleation and propagation. The main stages for corrosion-fatigue to occur are:

- initiation of minute corrosion pits,
- transition from pits to minute cracks,
- coalescence of minor cracks to form macro-cracks,
- final rupture of component.[54,58,101,107,108,113,114]

This is shown by the fracture surface analyses of a typical EA1N axle steel in Figure 11.[101] Under the action of cyclic stresses in the presence of a corrosive medium (rainwater), localized corrosion is initiated at susceptible sites, resulting in pits (white areas in Figure 11a).[54,95,101] The corrosive medium allows the transfer of electrons, resulting in corrosion and hence metal loss, creating the small pits (micro-cavities). Fewer pits were nucleated at the interface between the matrix and inclusions, whereas many more pits were nucleated within the ferrite grains and the ferrite-ferrite grain boundaries.[101] Corrosion pits were seldom found in the pearlite grains and within the ferrite-pearlite grain boundaries (Figure 12). Under continuous fluctuating stresses, these pits coalesced, resulting in the development of micro cracks, with some coalescing to form macro-cracks (Figure 11b). Thus, the typical pit-to-crack transition is driven by mechanical stresses, loading time and electrochemical reactions, and can be complex.[114]

The simultaneous action of the electrochemical reaction and coalesced micro-cracks causes growth (Figure 11c) generating primary (pits) and secondary

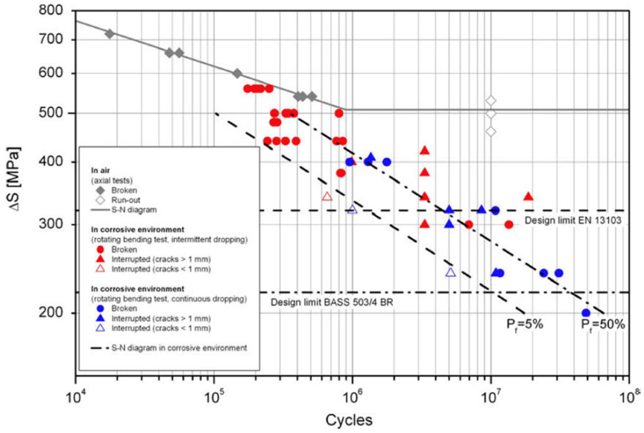

Figure 10. Comparison of S-N curves of typical rail axle steel tested in air and in corrosive environment.[54]

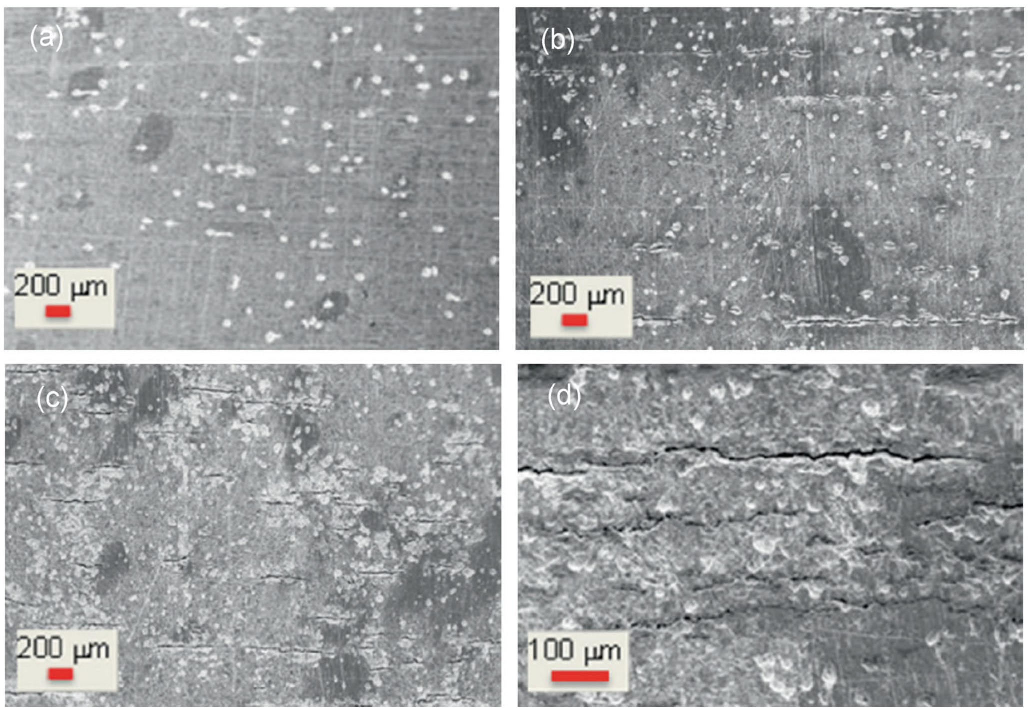

Figure 11. Corrosion fatigue pits-to-crack growth mechanism showing (a) initiation of pits from electrochemical action, (b) transition of pits to micro-cracks, (c) growth and coalescence of minute cracks and (d) macro-cracks on A1N rail axle steel.[101]

(coalesced micro-cracks) cracks. The primary and secondary cracks grow into each other under cyclic stresses, and the corrosion medium nucleates more minute pits. With growth, the coalesced micro-cracks became macro-cracks as shown in Figure 11d, demonstrating the pit-to-crack nucleation and propagation. The macro-cracks from the coalesced primary and secondary running in different directions can form "zig-zag" patterns.[54,101] Corrosion fatigue does not usually exhibit the "knee" (Figure 10) in a typical fatigue limit in air, due to the disappearance of the non-propagating crack which is critical for the crack closure mechanism.[115] The four transition stages associated with corrosion fatigue of EA4T rail axle steels are pit initiation, pit to crack transition, crack coalescence and final macro-crack rupture.[114]

3.2.1.3. Corrosion-fatigue crack growth models. The prediction of corrosion fatigue of typical rail axle steels from corrosion pits or micro-cavities is by the Hobson-Brown model (Equation 2).[116] This is the same relationship used for fatigue testing in air.[91]

$$\frac{da}{dN} = B(\boldsymbol{\Delta}\sigma)^{\beta} a^{n} \tag{2}$$

(2)where: B = materials constant, $\boldsymbol{\Delta}\sigma$ = stress range, β = materials constant, a = crack length and

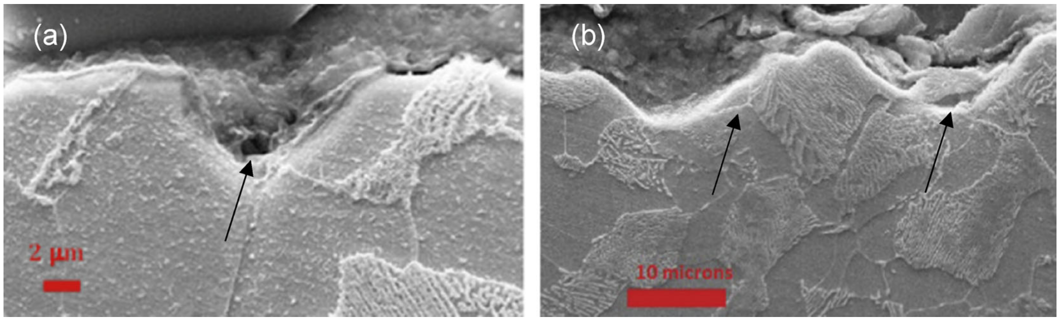

Figure 12. Ferrite-pearlite microstructure of EA1N rail axle steel showing: (a) corrosion pits initiated at the ferrite-ferrite grain boundaries and (b) pearlite colonies and grain boundaries surrounding corrosion pits initiated within ferrite grains and ferrite grain boundaries.[101]

n = materials constant. The material constants were extracted from crack propagation data.

The distribution of surface cracks during fatigue damage follows a typical Weibull statistical distribution function.[54,97] For typical small pits (less than the grain size), the S-N curve is estimated in terms of the propagation of cracks. As cracks nucleate from corrosion pits at different positions in the microstructure and propagate, they begin to grow and/or coalesce to form long cracks (few mm). This is shown in Equation 3 where the initial and final crack lengths are key parameters used to estimate the fatigue limit of the rail axle.

$$N_{prop} = \frac{1}{B(\Delta\sigma)^{\beta}} \int_{a_o}^{a_f} \frac{da}{a^n} \tag{3}$$

(3)where: a_o = average size of pit (initial length of crack), which are few microns, and a_f = final length of crack after micro-cracks coalesced.

Although Equation 3 has been used for corrosion fatigue life prediction of mechanical components including rail axles, it does not account for initial pit formation and the pit-to-crack transition.[52,91] However, it is at best expression of a median S-N curve for corrosion fatigue phenomenon.[52,54,88,97,99] To account for pit initiation and the pit-to-crack transitions, two models are used: modified Hobson-Brown [116] and the superposition models.[91] There are three main stages associated with the modified Hobson-Brown model (MHM): pit development, short fatigue crack growth rate and long fatigue crack growth rate. At the pit development stage, the relationship is given by Equation 4.

$$\left(\frac{da_p}{dN}\right)_p = C_p(a_t - a_p) \tag{4}$$

(4)where: C_p = pitting constant, a_t = pit to crack transition (µm) and a_p = pit length (µm). The pitting constant expressed in (Equation 5) is dependent on the corrosion environment and the specific alloy:

$$C_p = A_p(\Delta\gamma_t)^{\alpha_p} \tag{5}$$

(5)where: $\Delta\gamma_t$ = total shear strain range and A_p = material constant and α_p = constant that depends on the environment.

Once the corrosion pits nucleate, they act as stress concentration sites which can grow into cracks,[54,85,98] similar to a typical crack nucleated during fatigue tests in air. Corrosion fatigue for the short crack growth rate is estimated using Equation 6, and by integrating it with the upper and lower limits of d_m and a_t, the corrosion fatigue lifetime for short crack N_{sc} (subscript "sc" is short crack) can be estimated.

$$\left(\frac{da}{dN}\right)_{sc} = C_{sc}(d_i - a) \tag{6}$$

(6)where: $(da/dN)_{sc}$ = corrosion fatigue short crack growth rate (µm/cycles), $C_{sc} = G_i(\Delta\gamma_t)^b$, G_i and b = material constants, $\Delta\gamma_t$ = total shear strain range, d_i = grain size (varying from 60–120 µm for rail axle steel grades) and a = average crack length (µm).

Assessment of the long crack corrosion fatigue lifetime (N_{lc}) during corrosion fatigue is done by Equation 7, with the upper and lower limits being the grain sizes and the total crack length. Generally, the C_p, C_{sc} and C_{lc} constants are used to determine the growth rate and total corrosion fatigue life and are determined empirically based on pits/cracks at specific stress levels.

$$\left(\frac{da}{dN}\right)_{lc} = C_{lc}a \ \ - D \tag{7}$$

(7)where: $C_{lc} = B_{lc}(\Delta\gamma_t)^{\beta}_{lc}$ and $D = B_{lc}\left(\Delta\gamma_{fl}\right)^{\beta}_{lc} d_m$, $(da/dN)_{lc}$ = corrosion fatigue long crack growth rate (µm/cycles), D = threshold crack growth rate (µm/cycle), $\Delta\gamma_{fl}$ = fatigue limit total shear strain range (%), d_m = deceleration barrier length (µm), B_{lc} and β_{lc} = material-dependent constants. Evaluating the overall corrosion fatigue number of cycles required for

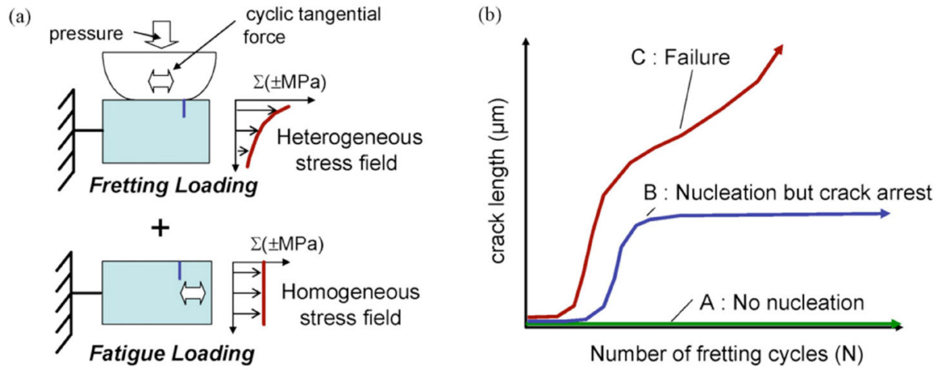

Figure 13. Schematic diagrams showing: (a) fretting and fatigue loading with heterogenous and homogenous stress fields and (b) the three main regimes and characteristics fretting-fatigue behavior.[125]

propagation of pit/crack is by the cumulative of lifetimes for the three stages as shown in Equation 8.

$$N_t = N_p + N_{sc} + N_{lc} \quad (8)$$

(8)where: N_p = pit development, N_{sc} = short crack growth and N_{lc} = long crack growth. The transition is from $a_0 \rightarrow a_t \rightarrow d_m \rightarrow a_f$.

Using the superposition model, corrosion fatigue can be estimated by the cumulative effect of fatigue crack growth in air and the effects of environment inducing the corrosion [EAC] behavior.[91] The driving force for fatigue crack growth rate in air is strain,[92,93,101,117] whereas for the EAC regime the driving force is the synergy between rail axle composition and the corrosive environment, hence is chemically driven.[103,106,114] Thus, environmentally assisted cracks are propagated beyond microstructural barriers such as grain boundaries, inclusions, and precipitates.[91]

3.2.2. Fretting fatigue failure overview

Fretting is the deterioration of surfaces subjected to repetitive and small relative motion.[118–121] It is the cold welding of asperities on the contacting surfaces and is enhanced by slip,[121–123] which breaks them further. The freshly exposed surfaces act as sites for crack nucleation, and these surfaces also undergo oxidation, leading to fretting corrosion. Fretting is complex and includes fretting fatigue, fretting wear and fretting corrosion.[124] Fretting fatigue failure is due to the simultaneous action of repetitive stresses on rail axle and localized stresses resulting from relative slip at the axle and wheel interface.[124,125] The depth of critical fretting damage for smooth and solid axles ranges between 200–250 μm in most European countries.[4,79,126,127] The loading process in fretting-fatigue is generally characterized by superposition of heterogenous fluctuating stress field (fretting loading) at the surfaces of the contacting components (i.e., axle and wheel assemblage) and the induced stress field resulting from cyclic stresses (Figure 13).[125] The evolution of crack damage is shown in Figure 13b as a function of the stress distribution. No cracks initiate below the fretting-fatigue threshold and the system is under the safe crack initiation condition (A in Figure 13b). For B in Figure 13b, initiation of crack is possible, although the cracks do not propagate due to reduced contact stresses at the contact interfaces. This is a typical safe crack arrest regime. For relatively high bulk fatigue loading and contact stresses, the nucleated cracks continue to propagate until final failure (C in Figure 13b), defining total failure or rupture regime.

The combined actions of stresses and slip contribute to reduce the fatigue strength.[125] Three main fretting fatigue modes are tension-tension (or tension-compression), bending and torsional fretting fatigue, Figure 14.[124] Fretting causes wear, formation of debris, and then crack propagation with reduced fatigue strength.[48,118,128–130] Fretting occurs at the pressed fits or interference fits on axles and can lead to catastrophic failure if not detected. Fretting fatigue is a main cause of failure of rail axles under rotation bending loads.[34,35]

3.2.2.1. Fretting maps.

A typical fretting map is given in Figure 15,[131] showing partial slip regime (PSR), mixed fretting regime (MFR) and gross slip regime (GSR) (also called slip regime (SR)).[125] The gross slip regime is also known as just slip regime.[124] The PSR, MFR and GSR are characteristic and dependent on material properties and the fretting conditions.[124,131] Thus, fatigue limits of rail axles due to fretting are much shorter than for typical "plain" fatigue under the same nominal bending stress amplitude.[124,132] In PSR, there is simultaneous abrasive and moderate oxidative wear occurring due to wear debris generated at

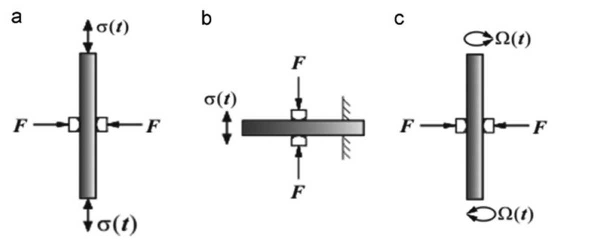

Figure 14. Fretting fatigue modes: (a) tension-tension (b) bending and (c) torsional fretting.[124]

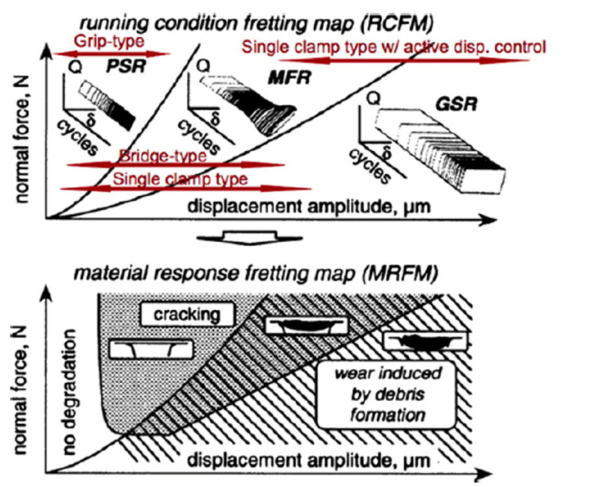

Figure 15. Typical fretting map showing fretting-fatigue wear mechanisms.[131]

the interference fit of the wheelset (region between the axle and wheel, which has different materials with different mechanical properties and microstructures).[132] For most alloys, the shortest fatigue lifetime with accompanying crack initiation and propagation occurs in the MFR. Within the GSR, the fatigue lifetime is higher than the MFR, but is not safe as it is close to the yield strength.

Typical fracture morphologies within the PSR, MFR and GSR for 7075 alloy are shown in Figure 16.[124] Within the PSR, very slight fretting scars were observed, whereas a very long crack at the boundary of the contact zone near the loaded area was observed in the MFR. In the GSR, severe wear zones were observed at the contact zones.

3.2.2.2. Fretting-fatigue predictive models. The main fretting-fatigue predictive models used for assessing mechanical properties of low carbon and high-strength low alloys are classical, fretting maps, plain fatigue, multiaxial fatigue, and fracture mechanics.[133–140] A typical empirical approach to estimating the fretting fatigue life of a mechanical component follows the process in Figure 17.[137] This combines fracture and damage mechanics approaches using strain constitutive equations (finite element modelling) with fracture mechanics crack propagation laws.[137] Fretting fatigue is complex, with four main locations for crack initiation and an empirical model should account for steep stress gradients, multiaxial stress states and non-linear bifurcaton. To address these, especially at the fretting fatigue crack initiation stage, various empirical models have been developed and modified as summarized in Figure 18 [132]. The four main approaches are continuum damage approach, stress invariant method, critical plane and applying fretting specific parameters.

The classical approach only uses empirical data such as nominal stresses, relative displacement of contacting surfaces and interfacial shear stresses to predict fretting fatigue life. A relationship between S-N curves and fatigue limit can be determined. The fatigue limit as a function of the reduction caused by fretting is given in Equation 9.[150] For wheelset, transition fillets between seat and axle body result in ~50% increase in overall fretting fatigue strength.

$$\sigma_{wf} = \sigma_{wo} - q\frac{8\mu P}{2\pi b} \qquad (9)$$

9where: σ_{wf} = fretting fatigue resistance, σ_{wo} = fatigue limit for plain specimen, q = notch sensitivity factor, P = contact force, μ = coefficient of friction and 2 b = width of the contact strip.

The main drawback of using the classical model is the inability to correlate all fatigue and fretting parameters,[52] which could lead to under- or overestimation of the fretting fatigue properties. This model is also difficult to use with other numerical models for fretting fatigue. The classical criteria and the fretting maps are useful for estimating the overall critical areas susceptible to fretting fatigue.

Fretting fatigue prediction based on plain fatigue approaches have been studied.[136–138,151] This is generally based on applying uniaxial plain fatigue test data, assuming the contact stress at the axle and wheel assembly is generally quasi-uniaxial. Generally, the Coffin-Manson low-cycle fatigue criterion (Equation 10) [152] is used to estimate the maximum strain amplitude and fretting fatigue limit.[52,151] The disadvantage is that the sensitivity of the parameters is materials dependent.

$$\varepsilon_{\max}, R_{\varepsilon} = C_1(N_f)^{C_2} + C_3(N_f)^{C_4} \qquad (10)$$

10where: $\varepsilon_{\max}$, R_{ε} = $\varepsilon_{\max}(1{-}R_{\varepsilon})^{m}$, C = fitting constant, N_f = fatigue life, $\varepsilon_{\max}$ = maximum strain amplitude along the contact interface, R_{ε} = strain ratio and m = fitting parameter. Equation 10 can be modified for multiaxial strain conditions.[52] Generally, the

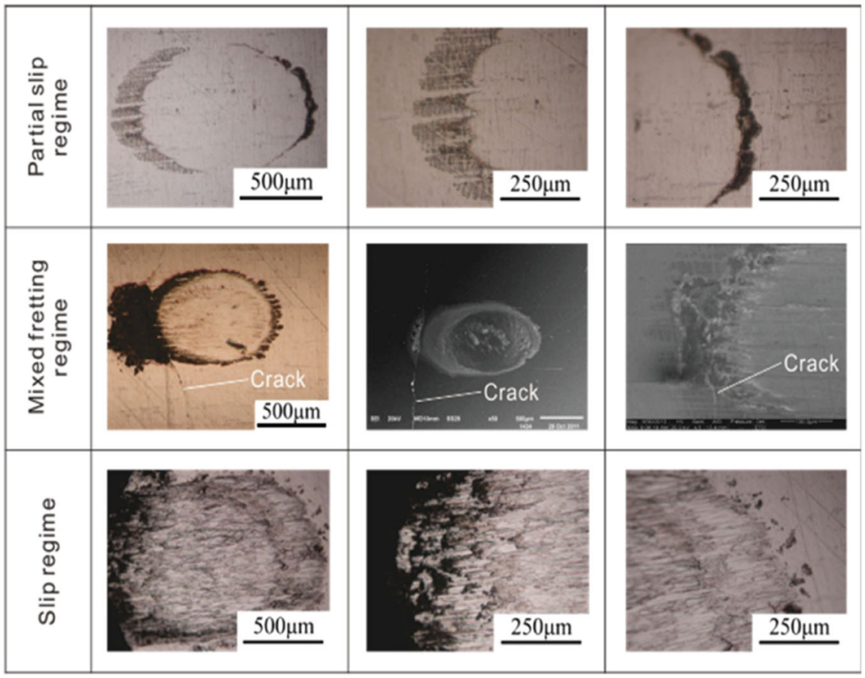

Figure 16. Fretting damage morphologies of Alloy 7075 showing the fretting running regime focusing on PSR, MFR and SR.[124]

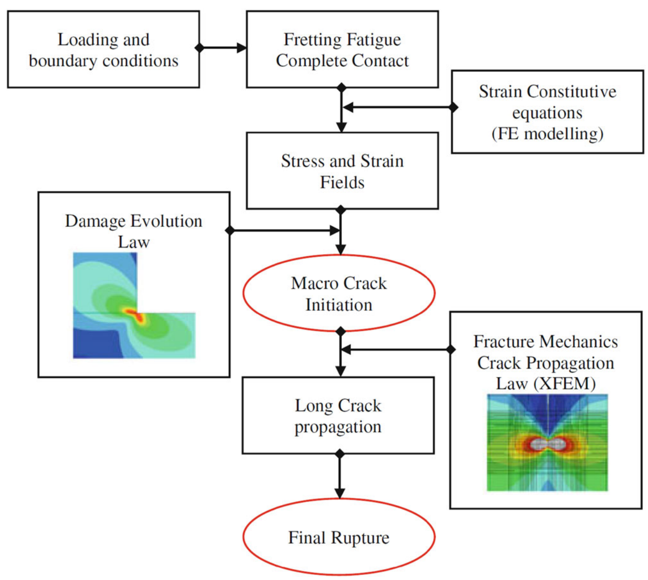

Figure 17. Total fretting fatigue lifetime prediction process flow chart.[137]

fretting fatigue life is estimated at a material-dependent distance from the stress concentration point. These continuum approaches describe fretting fatigue explicitly but do not have enough parameters to model fretting fatigue cracks.

3.2.2.3. Fretting-fatigue remedial actions. Surface engineering has been used to improve fretting corrosion resistance at ambient and higher temperatures.[35,153–155] Thermally sprayed Fe-Ni coatings on axles increased fatigue strength to 156 MPa from 103 MPa for uncoated axles.[35] The coating acts as a barrier, interrupting crack nucleation and propagation on the surface, improving the fretting resistance.[35,153–155] However, under rotating bending conditions, not all hard coatings improved fatigue limits, as cracks initiated beneath the coatings. Coatings with fine grains increase fatigue strength, as long as they do not have porosity.[154,156]

Induction hardening of the rail axles and wheels has greatly increased the resistance to fretting fatigue,[20] and has been done for rail axles used for the

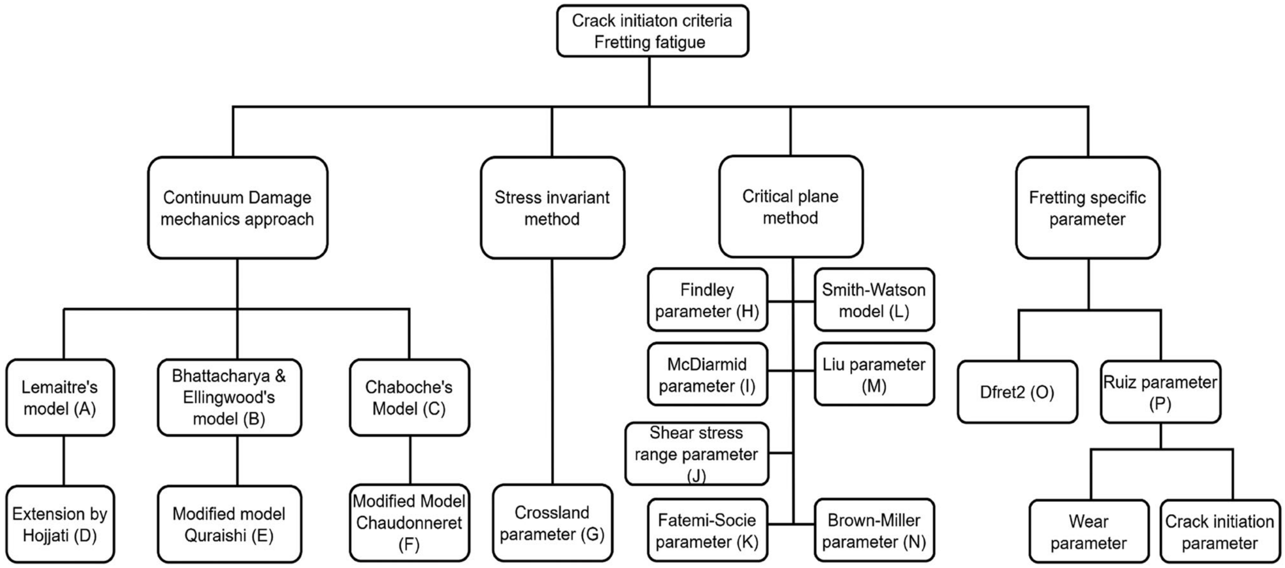

Figure 18. Parametric models applied to fretting fatigue crack initiation. The letters denote the references associated with specific models: A -,[133] B -,[134] C -,[135] D -,[136,137] E -,[138] F -,[139] G -,[140] H -,[141] I -,[142] J -,[143] K -,[144] L -,[145] M -,[146] N -,[147] O -,[148]P -.[149]

Japanese commuter and bullet trains. The disadvantage is that thermal stresses can induce cracking.

4. Steels for rail axles – chemistry and mechanical properties

The basic microstructures for rail axles were ferritic-pearlitic (Figure 19) ,[158,159] although more advanced alloy design produced other microstructures, especially with better manufacturing and increased understanding of the kinetics and thermodynamics influencing microstructures.[17,18,48,160] In ferrite-pearlite microstructures, smaller pearlite interlamellar spacing increases yield strength and UTS [99]. For typical ferrite-pearlite microstructure, the ferrite grain sizes ranges between 20–50 µm. Generally, allotriomorphic and Widmanstätten ferrite are observed for rail axle steels. With an axle of diameter of 180 mm, high hardness is observed at the surface which decreases to the core, because of the higher volume fraction of pearlite at the surface. Typical pearlite morphologies observed in rail axles that contribute to strength are given in Figure 20. These morphologies include granular, laminar (layered colonies that are oriented parallel to each other), tilted pearlite (differently oriented) and some secondary cementite.[161] The cementite lamellae of the granular pearlite are generally kinked, bent and fragmented to allow plastic deformation coordination of ferrite. This is mainly driven by thermal stresses from heat treatment and mechanical stresses and strain fields. The different morphologies and orientations are useful for improving strength since they provide different pathways for diverting and arresting cracks.

Many standards exist for the selection of steels for axles in Europe, Asia, North America, and Australia. The standards used in Europe are EN 13103[8] for non-powered axles, EN 13104[8] for powered axles and EN 13261[9] for typical axle requirements including material type, nondestructive testing and surface roughness tolerances. These standards served as benchmarks for the development of other alloyed steels. The Association of American Railroads (AAR) developed M101 for carbon steels,[17] India developed the ISR 16/95 standard, and Italy developed UN 16787-71 for steel axles. The American Society of Testing and Materials (ASTM) also recommended steel grade A730-99 for railway axles.

4.1. European grades (EN 13103 and EN13104)

Annex A of the European Standard EN 13261 has two grades of steels for manufacturing railway axles: EA1N and EA4T grades.[8,9,25,30,126,162,163] The EA1N grade (also known as C35) is a normalized low strength steel. The compositions of EA1N and EA4T grades are shown in Table 4. The pearlite colonies are distributed between ferrite grains of 20–40 µm.[170] Fatigue limit stresses were determined for ferrous alloys, and played a significant role in material selection and design.[20,170] The EA4T steel has better fatigue properties and lower notch sensitivity than EA1N steel, and hence is more widely used for axles. The EA1N steel grade is produced by vacuum degassing, then either forged or rolled into solid or hollow axles,[9] giving the properties shown in Table 5. The

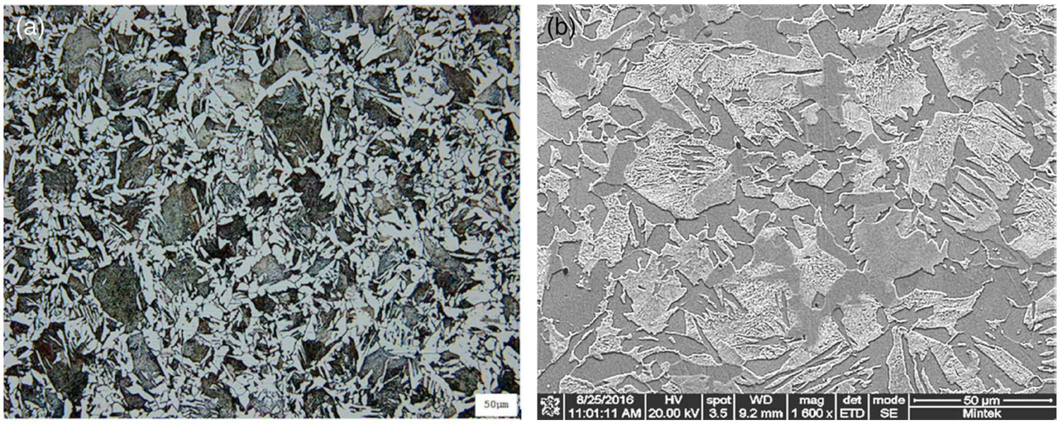

Figure 19. Microstructures of rail axle carbon steel showing ferrite (white) and pearlite (dark): (a) optical micrograph and (b) SEM image in secondary electron mode.[157]

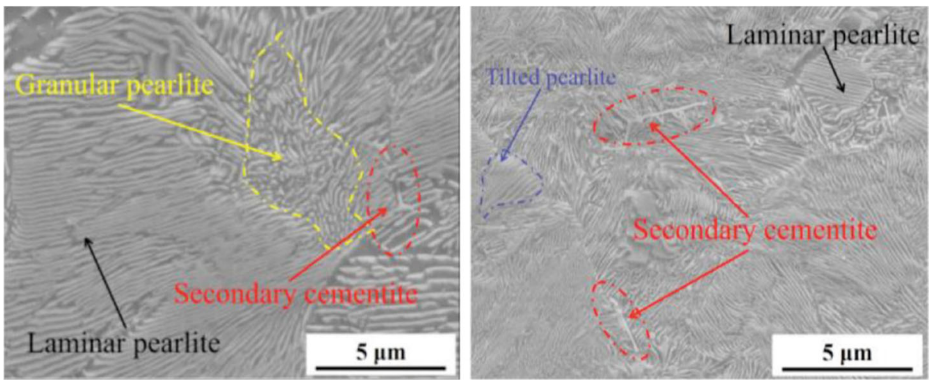

Figure 20. SEM-SE images showing different pearlite morphologies which are of the granular, tilted (differently orientated) and laminar (lamellar) types with some secondary cementite phases.[161]

Table 4. Composition of various axle materials.

	Composition (wt%)											
Alloy type	C	Si	P	S	Mn	Mo	Ni	Cr	Ti	V	Nb	Reference
Conventional European grade	0.37-0.38	0.15-0.46	0.04-0.05	0.04-0.05	1.12-1.20	0.05-0.06	0.05-0.06	0.3-0.4	–	0.05-0.06	–	8,9
MS3	0.29-0.30	0.63-0.70	0.02-0.03	0.02-0.03	1.54-1.60	–	–	–	0.02-0.03	0.10-0.30	–	164
MS6	0.19-0.20	0.34-0.35	0.02-0.03	0.01-0.02	1.32-1.40	–	–	–	–	0.11-0.20	–	
AAR	0.45-0.59	0.15	0.045	0.05	0.6-0.9	–	–	–	–	–	–	165
EA1N	0.40	0.50	0.02	0.02	1.20	0.08	0.30	0.30	–	0.06	–	166
EA4T	0.22-0.29	0.40	0.02	0.02	0.5-0.8	0.15-0.3	0.30	0.90-1.20	–	0.06	–	
35NiCrMoV12	0.26-0.32	0.40	0.02	0.015	0.40-0.70	0.40-0.60	2.70-3.30	0.60-1.00	–	0.08-0.13	–	
35CrMo	0.35	0.27	0.016	0.015	0.55	0.2	0.06	0.9	–	–	–	167,168
LZ50	0.47	0.26	0.014	0.01	0.78	–	0.028	0.02	–	–	–	169

Note: MS3 and MS6 alloys were designed in India for rail axles[164]. AAR grades are axle materials by Association of American Railroads and are mostly carbon steels. Grades EA1N and EA4T are used extensively in Europe for rail axle according to EN 13103/13104. Grade 35NiCrMoV12 is a HSLA steel.

fatigue limit stress of the EA1N is largely affected by grain size, texture, and phase distribution, which are influenced by alloy chemistry, mechanical working, and heat treatment.

Fatigue properties and characteristics are determined for correct dimensioning and designing to ensure structural integrity and optimum performance of the railway axle under in-service stresses.[8,9] The fatigue limits are estimated with reduced (axle geometry is not considered) and full-scale test pieces. Full scale railway axle testing is done under simulated environmental and stress states to assess worst case scenarios (maximum stresses). The results are used to estimate safety factors and possible conditions that the axle can be subjected to practice. Full scale testing is also used as verification and validation of calculated and permissible stress ranges referred to in EN 13103 and EN 13104 standards.[8,9]

The fatigue limits are also estimated for smooth (fatigue limit R_{fL}) and notched (fatigue limit R_{fE}) test

Table 5. Mechanical properties of rail axle steels.[8,9]

Steel	Yield strength (MPa)	Tensile strength (MPa)	Elongation (%)	longitudinal Charpy U-notch (J)	Transverse Charpy U-notch (J)
EA1N	≥320	550-650	≥22	≥30	≥20
EA4T	≥420	650-800	≥18	≥40	≥25

Table 6. Comparison of standard and typical rail axle steel fatigue limit values in EN 13261.[8,9,19]

Limit	Fatigue strength (solid axle) F_1 (MPa)	Fatigue strength (notched surface) F_2 (MPa)	Fatigue limit (smooth specimen) R_{fL} (MPa)	Fatigue limit (notched specimen) R_{fE} (MPa)	Notch sensitivity coefficient $q = R_{fL}/R_{fE}$
Standard	≥200	≥80	≥250	≥170	≤1.47
EA1N	≥200	≥80	≥250	≥170	≤1.47
EA4T	≥240	≥96	≥350	≥215	≤1.63
30NiCrMoV12	≥300	≥120	≥480	≥320	≤1.5

Table 7. Mechanical properties of the HSLA steel grade.[19]

Steel	Yield strength (R_e) (MPa)	Ultimate tensile strength (R_m) (MPa)	Elongation (%)	Impact toughness (longitudinal direction) (J)	Impact toughness (transverse direction) (J)
30NiCrMoV12	≥834	932-1079	≥15	≥47	≥22

pieces, as well as the surface of a solid axle (F_1) and the bore surface of hollow axle (F_2). Fatigue limits determined from reduced test pieces are used to determine the notch effect of the material, in accordance with security coefficient 'S', which is defined in EN 13103 and EN 13104 [8,9] and also to estimate the notch sensitivity coefficient (q) of the railway axle. These are used to determine maximum allowable stresses and safety factors, as damage tolerance.[171,172] Standard fatigue limit values for European standard axle steels are shown in Table 6. A minimal safety coefficient of 1.2 is expected for European axles in accordance with EN 13103 and 13104 standards, but the influence of dynamic stresses, torsion and vibrations on a driven axle could result in increased safety coefficients.[19] The fatigue limits of EA1N and EA4T axle steel are listed in Table 6. Although EA4T had better fatigue resistance, due to its high notch sensitivity, EA1N is the preferred grade.

4.2. High-strength low-alloyed (HSLA) steels for high-speed trains

High strength low-alloyed (HSLA) steels are used for manufacturing hollow axles for high-speed trains, especially 30NiCrMoV12 and 34CrNiMo6 in Europe.[19] Grade 30NiCrMoV12 steel is quenched and tempered, to give a mixed ferrite-pearlite microstructure with very high strength (Table 7). These grades were developed by Lucchini RS Company, Lovere, Italy, for rail applications according to standard UN 16787-71.[173] The compositions are given in Table 4. They have high fatigue strengths and notch sensitivity values. Axles produced from alloyed steel grade 30NiCrMoV12 had at least 20% weight reduced than EA4T, and about 30% less than EA1N.[166] This lightweight axle is achieved by hollow axle design, where the external diameter of the axles can be decreased. The mechanical properties of this grade of rail axle steel are shown in Table 7.[19]

Axles have been produced for high speed trains, e.g. the Italian Pendolino and the German Inter-City Express (ICE), using various grades of high strength low alloy steels such as 30NiCrMoV12 and 34CrNiMo6,[174,175] giving relatively high yield and ultimate tensile strengths. The high strength and hardness are improved by precipitation hardening and high amounts of retained austenite,[176] and allow hollow axle design, which is critical for light weighting to reduce the inertia moments for high speed trains.[166,170,175] These grades have no temper brittleness and retain useful machinability at relatively high hardnesses. Impact test results carried out at cryogenic temperatures (down to −125 °C) showed some ductility, while carbon steels are fragile below 0 °C.[177,178] The good cryogenic properties enabled the use of these steels in most Scandinavian countries. The fatigue characteristics of steel grade 30NiCrMoV12 are shown in Table 8, and are higher than most standard grades, e.g. EA4T steel, but they have similar notch sensitivity.[4]

4.3. Australian grades

Forged and rolled axle bars are mostly produced from AS 1448/K5 and AS 1442/5FG steel grades in Australia. The AS 1448/K5 grades are normalized or tempered carbon-manganese steels, giving a good

Table 8. Mechanical properties of various axle materials.

Steel grade	Yield strength (MPa)	UTS (MPa)	Elongation (%)	References
Conventional	320	550	22	8,9
MS3	400	700	21	164
MS6	404	625	22	
AAR	345	607	22	15
EA1N	320	550-650	22	8,9
EA4T	420	650-800	18	
35NiCrMoV12	600	800-950	13	19
30NiCrMoV12	860	975	20	
35CrMo	863	982	22	167,168
LZ50	330	629	24	169
AS1440/4340	770	980	14	20
SFA55	275	540	23	
SFA60/Q	295	590	20	
SFA65	345	640	23	
JIS S38C (AS10038)	294	539	25	179,180,181

combination of hardness, tensile strength, and tougher core than plain carbon steels, and so balance the tradeoff between strength and ductility. They are heat treated by surface flame or induction hardening. Most of these carbon-manganese steels are fully pearlitic, and typical compositions are shown in Table 4.

4.4. Association of American railroads (AAR) grades

Railway axles in North America are produced from carbon steels, according to the AAR M-101 standard specifications.[165] The specified mechanical properties include minimum UTS of 607 MPa, yield strength of 345 MPa with an elongation of 22% and about 37% reduction in area. Axles produced based on the AAR standard are mostly eutectoid carbon steels, with double normalizing and tempering, and were most of the axle steels.[15] The double normalizing and tempering heat treatment improved yield and tensile strengths,[15] with improved ductility.[15,182] The compositions according to AAR standard are listed in Table 4.

For ASTM standard A730-99, rail axles are also manufactured from alloy steels such as AISI 4140.[183] These axles are normalized, quenched, and tempered. Experimental AISI 4140 steels have a tensile strength of 860 MPa, yield strength at 725 MPa and with elongation and reduction in area at 18% and 50%.[183] Axles produced from ASTM standard A730-99 had better properties than the conventional grade based on the European standard.

4.5. Chinese steel grades

The Chinese have two main steel grades for rail axle production: LZ50 and 35CrMo rail axle steels with the compositions shown in Table 4.[167–169,184] The LZ50 grade is an alloyed medium carbon steel, with a microstructures of coarse ferrite and pearlite.[169,184] Axles are is normalized for 9000 seconds at 860 °C and then tempered for 5400 seconds for 575 °C.[130,184] The 35CrMo steel grade has a bainitic microstructure,[167,168] comprising very fine aggregates of ferrite and cementite. Axles made from the 35CrMo steel grade are austenitised at ~850 °C for 1800 seconds, quenched in oil, then tempered at 580 °C for 1800 seconds and finally air-cooled.[167,168]

4.6. Japanese grades

The Japanese railway axle grades are guided by the standards JIS E4502-2-2001 [179,180] for rolling stock and JRIS J0401-2007 [185] for induction-hardened axles for high-speed vehicles. The JIS E502 and JRIS J0401 standards specify axle classes, chemical compositions, mechanical properties, and manufacturing requirements. The JIS S38C (AISI 10038) is a medium carbon steel, which is quenched, tempered, and used for producing induction-hardened axles.[13] The improved chemical and mechanical properties are in the 2001 edition of JIS [179,180] and the 2007 edition of JRIS [185] standards. After forging and machining, axles are induction hardened, which induces compressive residual stresses, increasing fatigue strength.[13,97,186] Carbon steels grades that are also used for axles are SFA55, SFA60, SFA65 and SFAQA. The induction heat treatment of railway axles in Japan was initiated in the early 1960s also improves yield and tensile strengths, and toughness.[20]

4.7. Indian standard grades

The conventional steel grade used in India for railway axles is low carbon steel, although they have poor corrosion resistance.[164] Efforts to develop alloyed steels with improved mechanical and corrosion properties led to the development of the two alloy steels; MS3 and MS6 (Table 4) at the Kanpur Institute of

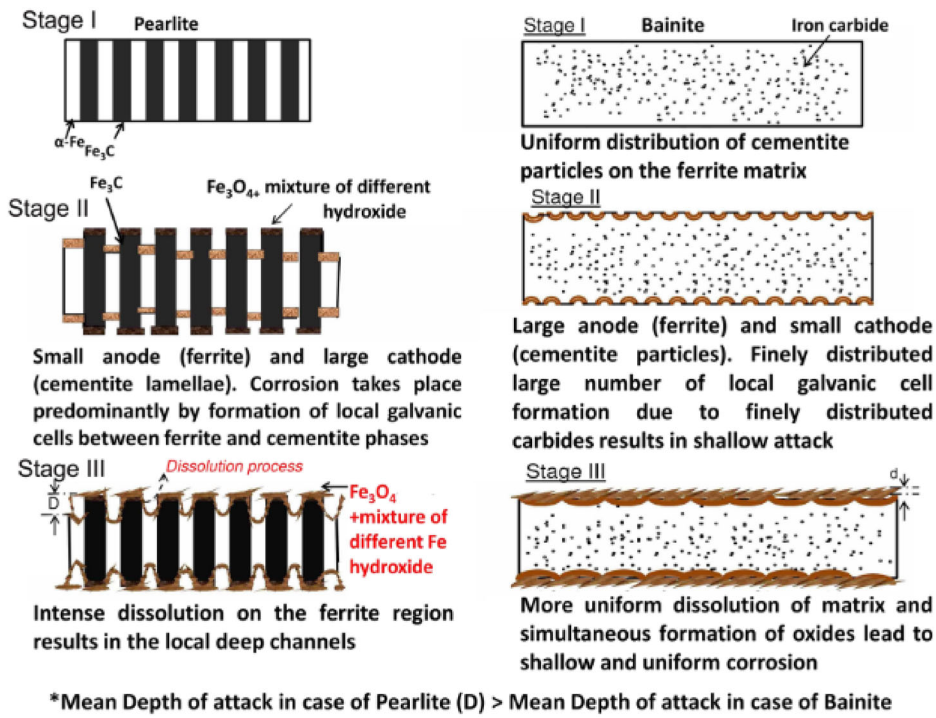

Figure 21. Corrosion mechanisms in pearlitic and bainitic steels with different stages of oxide formation.[190]

Technology in 2013.[164] The heat treatment is normalizing, and forged railway axles were produced according to the Indian Standard ISR16/95.

Electrochemical polarization and immersion tests conducted on MS3 and MS6 alloys in seawater (3.5% NaCl solution) revealed less pitting than for conventional alloys steels in India.[164] The corrosion rates of MS3 and MS6 alloys were lower than conventional axle steel grades although the microstructures were the same, which is ferrite-pearlite. For MS3 steel, the improved corrosion resistance was attributed to the formation of nano-sized SiO_4^{2-} ions, which promoted selective cation permeability reducing chloride ions penetration rates in the rust.[187] There was less pitting in the MS3 and MS6 due to the relatively high amounts of Mn, Si, and S than the conventional grade. The MnS inclusions are effective in reducing the formation of corrosion pits due to their poor conductivity, which reduces the ability to form corrosion cells in MS3 steel in chloride environments.[188,189]

Microstructure and alloying elements are important for corrosion resistance of steels (Figure 21).[164,190] Increased pearlite in ferrite-pearlite microstructures could increase metal dissolution rates.[191] Pearlite reduces the corrosion resistance of steels in chloride saturated environments, due to its high cementite proportions. For a ferrite-pearlite microstructure, there is small anode (ferrite) compared to a large cathode (cementite lamellae), which is the exact opposite of the ferrite-bainite microstructure. Generally, fine interlamellar spacings and fine pearlite colonies enhance corrosion resistance as observed for MS3 alloys.[164] A summary of the corrosion mechanism is shown in Figure 21. For a ferrite-pearlite microstructure, pearlite corrodes more easily resulting in high corrosion products. The corrosion products possess high induced stresses with associated volume expansion which leads to cracking.[191] The finer pearlite colonies and interlamellar spacings in MS3 alloys than in conventional alloys resulted in uniform stress distributions in the corrosion products, which were more stable than products with stress gradients,[164,190] and so had less cracking.

Low carbon contents decrease pearlite amounts, hence reducing its effect on corrosion. The MS3 alloys possess low carbon contents and finer interlamellar pearlite spacing, hence the improved corrosion resistance, which also promotes more uniformity in the stress distribution in the corrosion product than the conventional steel. High corrosion rates in the conventional steel were due to relatively high carbon content and coarse interlamellar spacing in the pearlite colonies. The Indian developed alloy MS3 and MS6 steels had improved corrosion resistance under fog, immersion, and polarization tests than conventional alloy steels, as well as improved mechanical properties.

Countries such as Egypt and South Africa have rail transport integrated into their transport network

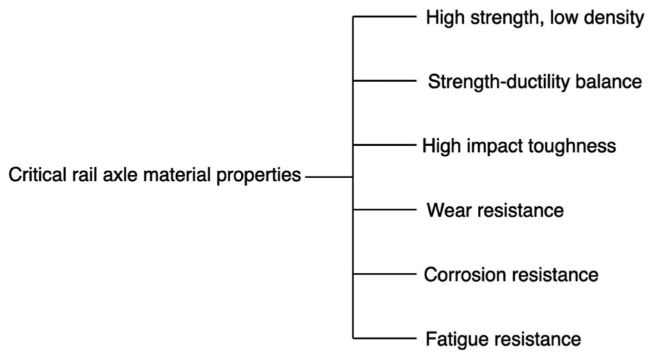

Figure 22. Critical mechanical properties of typical material for rail axles.

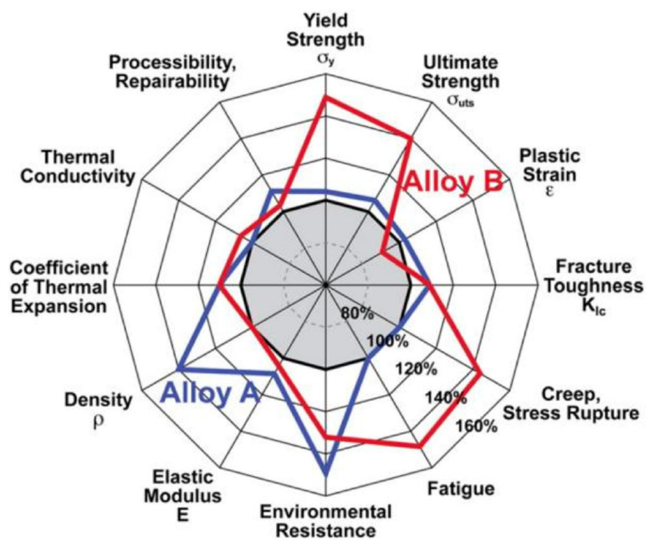

Figure 23. Spider web chart showing how improvement of new alloys are benchmarked against commercially available alloys.[193]

system. For example, South Africa has a Government Department of Science and Innovation, although most of their rail axle steel grades are proprietary. The steel grades being used there are comparable to most of the European Standards.

5. Areas for future research

Rail axle materials need to meet certain critical mechanical and physical properties to ensure structural integrity as summarized in Figure 22. These properties can be induced to rail axle material without increasing cost, by exploring low cost low density rail axle steels and coatings.[192] However, it is often difficult to improve all desired properties, and ductility could be compromised by increasing strength, Figure 23.[193] For a typical rail axle material, the grey polygon with the black outline shows the minimum property requirement or conventional grade, and any property should be above the minimum. Hypothetical Alloy A meets all the criteria although thermal conductivity and creep resistance are the same as the rail axle standard compositions. However, thermal conductivity and creep resistance are not critical requirements for rail axles, Figure 22. Hypothetical Alloy B has over 80% of its properties exceeding the conventional grade, but the critical requirement for axle material, plain strain. is very poor. Although Alloy B could be potential alloy, ways to improve the plain strain should be devised.

Limitations of the current rail axle steel grades are relatively low strength (∼300 MPa for yield strength and ∼600 MPa for UTS), poor corrosion resistance and comparative high density.[13,14,97,194] Generally, for most one main element alloy systems (where most of the constituents are dilute in concentration), strength and ductility are mutually exclusive; a gain in strength compromises ductility and toughness.[195] Light weight axles are also critical for development of trains of the future, to reduce both energy and material consumption,[196] to become enablers and drivers of an eco-friendly transportation system. Thus, other structural materials than steels could be considered, where better performance and mechanical properties would have to be traded for higher cost and greater reliability.[76,197–199]

There are many combinations of metallic materials which could fit the requirements for rail axle materials of the future.[112,181,186,196–204] However, the developments in computational materials design using machine learning (ML) and artificial intelligence systems could be advantageous to reduce the choices. The traditional Edisonian approaches have been expensive and designed and desired properties are not always met. Thus, ML combined with calculation of phase diagram (CALPHAD) techniques (e.g. Thermo-Calc) should be explored to define new classes of alloys by their phases to reduce time by identifying likely compositions quickly. Targeted alloy design could lead to solving light weighting and corrosion resistance requirements of future rail axle steels. Low density steels [205–207] and complex concentrated alloys [197–199,208–211] could be explored for potential rail axle materials.

"Complex concentrated alloys" (CCAs) are based on multiple principal elements with near equiatomic compositions. Alloys of this type could be developed to solve the strength-ductility tradeoff due to the simultaneous development and co-existence of strengthening and toughening mechanisms.[212–220] This is not the case in typical carbon steels used for rail axles where there is an inverse relationship between strength and ductility.[195] Some unique properties have been achieved for this new paradigm in alloy design using computational and experimental approaches at the nano [197–199,208,221–225] and micro-scales.[212,215,226–233] For example, the strength-ductility synergy is achievable due to the complementary effects of toughening and strengthening mechanisms. These mechanisms include solid solution strengthening, interstitial strengthening, dislocation interactions, transformation induced plasticity, twining induced plasticity, stacking faults, nano-precipitation and nano twinning.[234] It is generally difficult to have so many active mechanisms in conventional dilute alloys, hence the tradeoffs between properties.[195] Similarly, the equiatomic and non-equiatomic compositions of CCAs have high flexibility to design high strength and lightweight materials,[197–199,208,211,222] because different elements can be used, including lightweight alloying elements. Currently, research around CCAs is still developing and is based on the composition criterion, although very high cost implications could discourage their use.[198,208] Alloying elements such as Cr, Ni, Mo, V, Nb and Ru are very expensive and using them in very high quantities increases overall cost. This was the main reason why most expensive elements were used in minute proportions in one main element alloys to reduce cost.

Coating of rail axles using cold spraying should be explored for improved surface properties,[235–237] which would increase fatigue resistance, as well as corrosion resistance. Cold spraying does not require applied heat, so there are no phase transformations to change the microstructure as well as great potential for repair.[238,239] This technique has been successful for coatings on bulk titanium alloys,[240,241] aluminum alloys [242,243] and on complex concentrated alloys.[244,245] Cold sprayed coatings can enhance the mechanical properties at the axle surfaces, to reduce surface defects, and help prevent sites for corrosion and fatigue. The cold spraying equipment is not expensive, and the weight of the coatings increases the axle weight negligibly.

6. Summary and concluding remarks

Many railway axle failures are attributed to corrosion fatigue, where corrosion of the surface provides defects for surface crack nucleation, and inclusions could lead to sub-surface crack nucleation. However, most railway axles have not been designed for corrosion resistance because priority was on strength. Thus, corrosion resistance of many current axle materials is not satisfactory. This is due to the generally poor corrosion resistance of carbon steels used for rail axles, and ballast impact that generate micro surface defects. Corrosion and corrosion fatigue are the main precursors of surface defect induced axle failures. Coatings have been employed to reduce surface defects, although they can be detrimental if debonding or delamination wear occurs. However, recent advances in alloy development have included corrosion properties.

Finally, ways to improve efficiency and develop tools for enhanced structural integrity of rail axle materials such as coatings using cold spraying were highlighted. The need to explore complex concentrated alloy coating materials and techniques to enhance mechanical properties of rail axles was also suggested. The implication of these results on structural integrity of rail axles and areas for future research directions were discussed.

ORCID

D. E. P. Klenam http://orcid.org/0000-0003-1914-9633
L. H. Chown http://orcid.org/0000-0001-9699-6065
L. A. Cornish http://orcid.org/0000-0002-9291-4584

References

1. Robinson, M.; Kapoor, A. *Fatigue in Railway Infrastructure*; Woodhead Publishing Limited, CRC Press, Great Abington, Cambridge, UK, 2009.

2. Molemaker, R.; Pauer, A. *The Economic Footprint of Railway Transport in Europe*, Community of European Railway, ECORYS Brussels, Belgium, 2014.
3. Human Development Report. *Sustaining Human Progress: Reducing Vulnerabilities and Building Resilience*, United Nations Development Program, New York, USA, 2014.
4. Luke, M.; Varfolomeev, I.; Lütkepohl, K.; Esderts, A. Fatigue Crack Growth in Railway Axles: Assessment Concept and Validation Tests. *Eng. Fract. Mech.* 2011, *78*, 714–730. doi:10.1016/j.engfracmech.2010.11.024
5. Smith, R. A.; Hillmansen, S. A Brief Historical Overview of the Fatigue of Railway Axles. *Proc. Inst. Mech. Eng. Part F J. Rail Rapid Transit.* 2004, *218*, 267–277. doi:10.1243/0954409043125932
6. Zerbst, U.; Beretta, S.; Köhler, G.; Lawton, A.; Vormwald, M.; Beier, H.; Klinger, C.; Černý, I.; Rudlin, J.; Heckel, T.; et al. Safe Life and Damage Tolerance Aspects of Railway axles - A Review. *Eng. Fract. Mech.* 2013, *98*, 214–271. doi:10.1016/j.engfracmech.2012.09.029
7. Hillmansen, S. Editorial to the Special Issue on Railway Axles. *Proc. Inst. Mech. Eng. Part F J. Rail Rapid Transit.* 2004, *218*, I–II. doi:10.1177/095440970421800401
8. European Standard. *EN 13103. Railway Applications - Wheelsets and Bogies - Non Powered Axles - Design Method. European Committee for Standardization (CEN)*, Brussels, Belgium, 2001.
9. European Standard. *EN 13261. Railway applications - Wheelsets and bogies - Axles - Product Requirement, Annex A. European Committee for Standardization (CEN)*, Brussels, Belgium, 2003.
10. Yao, Z.; Dai, W.; Cai, B.; Li, C.; Zhang, H.; Zhang, Y. Effect of Quenching Temperature on Tensile Strength and Fatigue Behavior of an EA4T Steel. *J. Mater. Eng. Perform.* 2021, *30*, 9015–9028. doi:10.1007/s11665-021-06117-0
11. Nwe, T.; Pimsarn, M. Railway Axle and Wheel Assembly Press-Fitting Force Characteristics and Holding Torque Capacity. *Appl. Sci.* 2021, *11*, 1–16.
12. Pourheidar, A.; Patriarca, L.; Beretta, S.; Regazzi, D. Investigation of Fatigue Crack Growth in Full-Scale Railway Axles Subjected to Service Load Spectra: Experiments and Predictive Models. *Metals (Basel)* 2021, *11*, 1427. doi:10.3390/met11091427
13. Gao, J.-W.; Yu, M.-H.; Liao, D.; Zhu, S.-P.; Zhu, Z.-Y.; Han, J. Foreign Object Damage Tolerance and Fatigue Analysis of Induction Hardened S38C Axles. *Mater. Des.* 2021, *202*, 109488. doi:10.1016/j.matdes.2021.109488
14. Asngali, B.; et al. Static Analysis of Railway Axle Using Finite Element Method and Monitoring of Railway Bearing Based on Vibration Analysis. *J. Phys. Conf. Ser.* 2021, *1845*, 012037.
15. Lonsdale, C.; Stone, D. North American Axle Failure Experience. *Proc. Inst. Mech. Eng. Part F J. Rail Rapid Transit.* 2004, *218*, 293–298. doi:10.1243/0954409043125941
16. Lonsdale, C.; Dedmon, S.; Galbraith, J.; Pilch, J. 2007 Recent Research to Improve Wheel and Axle Composition, Properties and Designs. In *ASME 2007 Rail Transportation Division Fall Technical Conference*. ASME; pp 13–20. doi:10.1115/RTDF2007-46008
17. Association of American Railroads. *Manual of Standards and Recommended Practices - Section G, Wheels and Axles, Specification M107/208, "Wheels, Carbon Steels*. The Association of American Railroads, Washington DC, USA, 2007.
18. Japanese Standards Association. *Axles for Railway Rolling Stock, Japanese Industrial Standard E, 4502*, Tokyo, Japan, 1989, 1–4.
19. Novosad, M.; Fajkoš, R.; Řeha, B.; Řezníček, R. Fatigue Tests of Railway Axles. *Proc. Eng.* 2010, *2*, 2259–2268. doi:10.1016/j.proeng.2010.03.242
20. Hirakawa, K.; Toyama, K.; Kubota, M. The Analysis and Prevention of Failure in Railway Axles. *Int. J. Fatigue* 1998, *20*, 135–144. doi:10.1016/S0142-1123(97)00096-0
21. Cantini, S.; Beretta, S. *Structural Reliability Assessment of Railway Axles*. Series LRS-Techno Lucchini RS, Lucchini RS Publishers, Italy, 2011, 4, 1–207.
22. Japanese Industrial Standards. *Standard E4501. Railway Rolling Stock - Design Method for Strength of Axles*, 1995.
23. Lundén, R.; Vernersson, T.; Ekberg, A. Railway Axle Design: To Be Based on Fatigue Initiation or Crack Propagation? *Proc. Inst. Mech. Eng. Part F J. Rail Rapid Transit.* 2010, *224*, 445–453. doi:10.1243/09544097JRRT384
24. Zerbst, U.; Schödel, M.; Beier, H. T. Parameters Affecting the Damage Tolerance Behaviour of Railway Axles. *Eng. Fract. Mech.* 2011, *78*, 793–809. doi:10.1016/j.engfracmech.2010.03.013
25. Zerbst, U.; Klinger, C.; Klingbeil, D. Structural Assessment of Railway Axles – a Critical Review. *Eng. Fail. Anal.* 2013, *35*, 54–65. doi:10.1016/j.engfailanal.2012.11.007
26. Grubisic, V.; Fischer, G. Procedure for Reliable Durability Validation of Train Axles. *Materialwissenschaft und Werkstofftechnik: Entwicklung, Fertigung, Prüfung, Eigenschaften und Anwendungen technischer Werkstoffe.* 2006, *37*, 973–982. doi:10.1002/mawe.200600086
27. PRC Rail Consulting Ltd. Bogies and locomotive axle specifications. http://www.railway-technical.com/trains/rolling-stock-index-l/bogies.html.
28. Costa, P. J. F. *Fatigue Reliability Analysis of a Rail Vehicle Axle*; MSc Dissertation, Faculty of Engineering, Universidade of Porto, Portugal, 2020.
29. Zerbst, U.; Mädler, K.; Hintze, H. Fracture Mechanics in Railway Applications––An Overview. *Eng. Fract. Mech.* 2005, *72*, 163–194. doi:10.1016/j.engfracmech.2003.11.010
30. Klingbeil, D.; Zerbst, U.; Klinger, C. 2013 Safe and Damage Tolerance Concepts of Railway Axles. In *13th International Conference on Fracture.*
31. Zerbst, U.; Klinger, C.; Clegg, R. Fracture Mechanics as a Tool in Failure Analysis — Prospects and Limitations. *Eng. Fail. Anal.* 2015, *55*, 376–410. doi:10.1016/j.engfailanal.2015.07.001

32. Zerbst, U.; Lundén, R.; Edel, K.-O. O.; Smith, R. A. A. Introduction to the Damage Tolerance Behaviour of Railway Rails - a Review. *Eng. Fract. Mech.* 2009, *76*, 2563–2601. doi:10.1016/j.engfracmech.2009.09.003
33. Zerbst, U.; Beretta, S. Failure and Damage Tolerance Aspects of Railway Components. *Eng. Fail. Anal.* 2011, *18*, 534–542. doi:10.1016/j.engfailanal.2010.06.001
34. Gao, S.; Budde, L. Mechanism of Mechanical Press Joining. *Int. J. Mach. Tools Manuf.* 1994, *34*, 641–657. doi:10.1016/0890-6955(94)90049-3
35. Liu, W.; Xia, H.; Liu, Y.; Song, Z.; Xu, X. The Performances of a Thermally Sprayed Fe/Ni Composite Coating to Resist Fretting Fatigue under Rotational Bending Loads. *Surf. Coatings Technol.* 2013, *217*, 58–63. doi:10.1016/j.surfcoat.2012.11.072
36. Fec, M. C.; Moyar, G. J. Railroad Journal Roller Bearing Failure and Detection: Past, Present and Future. In *The American Society of Mechanical Engineers' Winter Annual Meeting*, 1988, pp 3–16.
37. Williams, S.; Ahlbeck, D.; Harrison, H. Railroad Bearing Performance under the Wheel Impact Load Environment. In *The American Society of Mechanical Engineers' Winter Annual Meeting*, 1988, pp 63–71.
38. Symonds, N.; Corni, I.; Wood, R. J. K.; Wasenczuk, A.; Vincent, D. Observing Early Stage Rail Axle Bearing Damage. *Eng. Fail. Anal.* 2015, 56, 216–232.
39. Corni, I.; Symonds, N.; Birrell, C. E.; Katsamenis, O. L.; Wasenczuk, A.; Vincent, D. Characterization and Mapping of Rolling Contact Fatigue in Rail-Axle Bearings. *Eng. Fail. Anal.* 2017, *82*, 617–630. doi:10.1016/j.engfailanal.2017.04.012
40. Locovei, C.; Răduță, A.; Nicoară, M.; Cucuruz, L. R. Analysis of Fatigue Fracture of Tank Wagon Railway Axles. In *Proceedings of the 3rd WSEAS International Conference on Finite Differences - Finite Elements - Finite Volumes - Boundary Elements*, 2010, pp 219–223.
41. Raduta, A.; Locovei, C.; Nicoara, M.; Cucuruz, L. R. On the Influence of Residual Stresses on Fatigue Fracture of Railway Axles. *WSEAS Trans. Appl. Theor. Mech.* 2010, *3*, 198–207.
42. Grubisic, V.; Fischer, G. (2006). Procedure for reliable durability validation of train axles. *Materialwissenschaft und Werkstofftechnik: Entwicklung, Fertigung, Prüfung, Eigenschaften und Anwendungen technischer Werkstoffe*, *37*(12), 973–982.
43. European Railway Agency. Railway Safety Performance in the European Union. http://www.era.europa.eu/Document-Register/Pages/Railway-Safety-Performance-in-the-European-Union-2011.aspx. 2011.
44. Orringer, O.; Morris, J. M.; Steele, R. K. Applied Research on Rail Fatigue and Fracture in the United States. *Theor. Appl. Fract. Mech.* 1984, *1*, 23–49. doi:10.1016/0167-8442(84)90019-3
45. Transportation Safety Board of Canada. *Railway Investigation Report R01Q0010*. Main track derailment. Trudel, Quebec, February 15, 2001. http://www.tsb.gc.ca/eng/rapports-reports/rail/2001/r01q001/r01q0010.asp.
46. Grubisic, V.; Fischer, G. Railway Axle Failures and Durability Validation. *Proc. Inst. Mech. Eng. Part F J. Rail Rapid Transit.* 2012, *226*, 518–529. doi:10.1177/0954409712442325
47. Hirakawa, K. Fatigue Design Method of Railway Axle in the High-Speed Railway. *Jpn. Railway Eng. Assoc.* 1996, *39*, 4–12.
48. Linhart, V.; Černý, I. An Effect of Strength of Railway Axle Steels on Fatigue Resistance under Press Fit. *Eng. Fract. Mech.* 2011, *78*, 731–741. doi:10.1016/j.engfracmech.2010.11.023
49. Hirakawa, K.; Kubota, M. On the Fatigue Design Method for High-Speed Railway Axles. *Proc. Inst. Mech. Eng. Part F J. Rail Rapid Transit.* 2001, *215*, 73–82. doi:10.1243/0954409011531413
50. Makino, T.; Kato, T.; Hirakawa, K. Review of the Fatigue Damage Tolerance of High-Speed Railway Axles in Japan. *Eng. Fract. Mech.* 2011, *78*, 810–825. doi:10.1016/j.engfracmech.2009.12.013
51. Clyne, T. W.; Gill, S. C. Residual Stresses in Thermal Spray Coatings and Their Effect on Interfacial Adhesion: A Review of Recent Work. *J. Therm. Spray Technol.* 1996, *5*, 401–418. doi:10.1007/BF02645271
52. Ekberg, A. Fretting Fatigue of Railway Axles - a Review of Predictive Methods and an Outline of a Finite Element Model. *IMechE J. Rail Rapid Transit.* 2004, *218*, 299–316. doi:10.1243/0954409043125905
53. Brister, S. E.; Dahlman, G. E.; Stecyk, N. J. Improving Axle Reliability in North American Freight Service. In *Proceedings of the 2006 ASME/IEEE Joint Rail Conference*, 2006.
54. Beretta, S.; Carboni, M.; Fiore, G.; Lo Conte, A. Corrosion–Fatigue of A1N Railway Axle Steel Exposed to Rainwater. *Int. J. Fatigue* 2010, *32*, 952–961. doi:10.1016/j.ijfatigue.2009.08.003
55. Gravier, N.; Viet, J. J.; Leluan, A. Predicting the Life of Railway Vehicle Axles. In *Proceedings of the 12th International Wheelset Congress*, 1998; pp 133–146.
56. Beretta, S.; Ghidini, A.; Lombardo, F. Fracture Mechanics and Scale Effects in the Fatigue of Railway Axles. *Eng. Fract. Mech.* 2005, *72*, 195–208. doi:10.1016/j.engfracmech.2003.12.011
57. Broek, D. The Practice of Damage Tolerance Analysis. ASM International, Materials Park, OH 44073-0002, USA, 1996, 420–426.
58. Schijve, J. *Fatigue of Structures and Materials*. Kluwer Academic Publishers, Springer, Amsterdam, Netherlands; 2004.
59. Snell, J. R. Key Issues in the Application of Unified Railway Axle Standards. *Proc. Inst. Mech. Eng. Part F J. Rail Rapid Transit.* 2004, *218*, 279–282. doi:10.1243/0954409043125914
60. Madia, M.; Beretta, S.; Zerbst, U. An Investigation on the Influence of Rotary Bending and Press Fitting on Stress Intensity Factors and Fatigue Crack Growth in Railway Axles. *Eng. Fract. Mech.* 2008, *75*, 1906–1920. doi:10.1016/j.engfracmech.2007.08.015
61. Watson, A. S.; Timmis, K. A Method of Estimating Railway Axle Stress Spectra. *Eng. Fract. Mech.* 2011, *78*, 836–847. doi:10.1016/j.engfracmech.2009.12.001

62. Ognjanovic, M.; Simonovic, A.; Ristivojevic, M.; Lazovic, T. Research of Rail Traction Shafts and Axles Fractures towards Impact of Service Conditions and Fatigue Damage Accumulation. *Eng. Fail. Anal.* 2010, *17*, 1560–1571. doi:10.1016/j.engfailanal.2010.06.007
63. Wells, J. H. Kinetic Boundary Friction. The Engineer, London, UK; 1929, 147, 454.
64. Hartog, J. P. D. Forced Vibrations with Combined Viscous and Coulomb Damping. *Philos. Mag.* 1930, *9*, 801–817. doi:10.1080/14786443008565051
65. Eadie, D. T.; Kalousek, J.; Chiddick, K. C. The Role of High Positive Friction (HPF) Modifier in the Control of Short Pitch Corrugations and Related Phenomena. *Wear* 2002, *253*, 185–192. doi:10.1016/S0043-1648(02)00098-4
66. Withers, P. J.; Turski, M.; Edwards, L.; Bouchard, P. J.; Buttle, D. J. Recent Advances in Residual Stress Measurement. *Int. J. Press. Vessel. Pip.* 2008, *85*, 118–127. doi:10.1016/j.ijpvp.2007.10.007
67. Withers, P. J.; Bhadeshia, H. K. D. H. Residual Stress Part 1 – Measurement Techniques. *Mater. Sci. Technol.* 2001, *17*, 355–365. doi:10.1179/026708301101509980
68. Klinger, C.; Bettge, D. Axle Fracture of an ICE3 High Speed Train. *Eng. Fail. Anal.* 2013, *35*, 66–81. doi:10.1016/j.engfailanal.2012.11.008
69. Danks, D.; Clayton, P. Comparison of the Wear Process for Eutectoid Rail Steels: Field and Laboratory Tests. *Wear* 1987, *120*, 233–250. doi:10.1016/0043-1648(87)90069-X
70. Beretta, S.; Carboni, M.; Lo Conte, A.; Palermo, E. An Investigation of the Effects of Corrosion on the Fatigue Strength of AlN Axle Steel. *Proc. Inst. Mech. Eng. Part F J. Rail Rapid Transit.* 2008, *222*, 129–143. doi:10.1243/09544097JRRT157
71. Dhua, S. K.; Ray, A.; Sarma, D. S. Effect of Tempering Temperatures on the Mechanical Properties and Microstructures of HSLA-100 Type Copper-Bearing Steels. *Mater. Sci. Eng. A* 2001, *318*, 197–210. doi:10.1016/S0921-5093(01)01259-X
72. Talamba, R.; Stoica, M. Mounted Axles. Rosia Montata, ASAB Dacia Publishing House, Bucharest, Romania 2005, ISBN 973-7725-04-2.
73. Wohler, A. Theorie Rechteckiger Eiserner Bruckenbalken Mit Gittetwanden Und Mit Blechwanden. *Zeitschrift Fur Bauwes* 1855, *5*, 121–166.
74. Ewing, J. A.; Humfrey, J. C. W. The Fracture of Metals under Repeated Alternations of Stresses. *Philos. Trans. R. Soc.* 1903, 200, 241–250.
75. Ritchie, R. O. Mechanism of Fatigue-Crack Propagation in Ductile and Brittle Materials. *Int. J. Fract.* 1999, *100*, 55–83. doi:10.1023/A:1018655917051
76. Klenam, D. E. P.; Soboyejo, W. O. Fatigue of Thermostructural Alloys. In *Reference Module in Materials Science and Materials Engineering*; Elsevier, Philadelphia, USA, 2022. doi:10.1016/B978-0-12-822944-6.00092-X
77. Klenam, D. E. P.; Oghenevweta, J. E.; Soboyejo, W. O. Fracture and Toughening of Intermetallics. In *Reference Module in Materials Science and Materials Engineering*; Elsevier, Philadelphia, USA, 2022. doi:10.1016/B978-0-12-822944-6.00070-0
78. Klenam, D. E. P.; Oghenevweta, J. E.; Soboyejo, W. O. Fatigue of Single/Multiple Semi-Elliptical Cracks. In *Reference Module in Materials Science and Materials Engineering*; Elsevier, Philadelphia, USA, 2022. doi:10.1016/B978-0-12-822944-6.00084-0
79. Schmidová, E.; Paščenko, P.; Culek, B.; Schmid, M. Premature Failures of Railway Axles after Repeated Pressing. *Eng. Fail. Anal.* 2021, *123*, 105253. doi:10.1016/j.engfailanal.2021.105253
80. Gürer, G.; Gür, C. H. H. Failure Analysis of Fretting Fatigue Initiation and Growth on Railway Axle Press-Fits. *Eng. Fail. Anal.* 2018, *84*, 151–166. doi:10.1016/j.engfailanal.2017.06.054
81. Axle, R.; et al. The Effects of Friction Coefficient and Interference on the Fretting Fatigue Strength of Railway Axle Assembly. *UPB Sci. Bull. Ser. D Mech. Eng.* 2013, *75*, 71–84.
82. Berthier, Y.; Vincent, L.; Godet, M. Fretting Fatigue and Fretting Wear. *Tribol. Int.* 1989, *22*, 235–242. doi:10.1016/0301-679X(89)90081-9
83. Stone, D. H. 2011 Fretting Fatigue of Axles. In *ASME 2011 Rail Transportation Division Fall Technical Conference*; pp 35–37.
84. Kappes, W.; Hentschel, D.; Oelschlägel, T. Potential Improvements of the Presently Applied in-Service Inspection of Wheelset Axles. *Int. J. Fatigue* 2016, *86*, 64–76. doi:10.1016/j.ijfatigue.2015.08.014
85. Zerbst, U.; Madia, M.; Klinger, C.; Bettge, D.; Murakami, Y. Defects as a Root Cause of Fatigue Failure of Metallic Components. I: Basic Aspects. *Eng. Fail. Anal.* 2019, *98*, 228–239. doi:10.1016/j.engfailanal.2019.01.054
86. Hillmansen, S.; Smith, R. A. The Management of Fatigue Crack Growth in Railway Axles. *J. Rail Rapid Transp.* 2004, *218*, 327–336. doi:10.1243/0954409043125879
87. Indraratna, B.; Ionescu, D.; Christie, H. D. Shear Behaviour of Railway Ballast Based on Large Scale Triaxial Testing. *J. Geotech. Geoenviron. Eng.* 1998, *124*, 439–449. doi:10.1061/(ASCE)1090-0241(1998)124:5(439)
88. Ren, X.; Wu, F.; Xiao, F.; Jiang, B. Corrosion Induced Fatigue Failure of Railway Wheels. *Eng. Fail. Anal.* 2015, *55*, 300–316. doi:10.1016/j.engfailanal.2015.06.009
89. Beretta, S.; Carboni, M.; Conte, A. L.; Regazzi, D.; Trasatti, S.; Rizzi, M. Crack Growth Studies in Railway Axles under Corrosion Fatigue: Full-Scale Experiments and Model Validation. *Proc. Eng.* 2011, *10*, 3650–3655. doi:10.1016/j.proeng.2011.04.601
90. Cervello, S. Fatigue Properties of Railway Axles: New Results of Full-Scale Specimens from Euraxles Project. *Int. J. Fatigue* 2016, *86*, 2–12. doi:10.1016/j.ijfatigue.2015.11.028
91. Murtaza, G.; Akid, R. Empirical Corrosion Fatigue Life Prediction Models of a High Strength Steel. *Eng. Fract. Mech.* 2000, *67*, 461–474. doi:10.1016/S0013-7944(00)00057-6

92. Alp, T.; Husain, Z.; Cottis, R. A. Corrosion Fatigue Crack Initiation and Growth in 18 Ni Maraging Steel. J. Mater. Sci. 1986, *21*, 9, 3263–3268.
93. Ragab, A.; Alawi, H.; Sorein, K. Corrosion Fatigue of Steel in Various Aqueous Environments. *Fat. Frac. Eng. Mat. Struct.* 1989, *12*, 469–479. doi:10.1111/j.1460-2695.1989.tb00557.x
94. Domínguez Almaraz, G. M.; Ávila Ambriz, J. L.; Cadenas Calderón, E. Fatigue Endurance and Crack Propagation under Rotating Bending Fatigue Tests on Aluminum Alloy AISI 6063-T5 with Controlled Corrosion Attack. *Eng. Fract. Mech.* 2012, *93*, 119–131. doi:10.1016/j.engfracmech.2012.06.012
95. Balbín, J. A.; Chaves, V.; Larrosa, N. O. Pit to Crack Transition and corrosion fatigue Lifetime Reduction Estimations by Means of a Short Crack Microstructural Model. *Corros. Sci* 2021, *180*, 109171. doi:10.1016/j.corsci.2020.109171
96. Chan, K. S. Roles of Microstructure in Fatigue Crack Initiation. *Int. J. Fatigue* 2010, *32*, 1428–1447. doi:10.1016/j.ijfatigue.2009.10.005
97. Hu, Y.; Wu, S.; Withers, P. J.; Cao, H.; Chen, P.; Zhang, Y.; Shen, Z.; Vojtek, T.; Hutař, P. Corrosion Fatigue Lifetime Assessment of High-Speed Railway Axle EA4T Steel with Artificial Scratch. *Eng. Fract. Mech.* 2021, *245*, 107588. doi:10.1016/j.engfracmech.2021.107588
98. Zerbst, U.; Madia, M.; Klinger, C.; Bettge, D.; Murakami, Y. Defects as a Root Cause of Fatigue Failure of Metallic Components. III: Cavities, Dents, Corrosion Pits, Scratches. *Eng. Fail. Anal.* 2019, *97*, 759–776. doi:10.1016/j.engfailanal.2019.01.034
99. Pineau, A.; McDowell, D. L.; Busso, E. P.; Antolovich, S. D. Failure of Metals II: Fatigue. *Acta Mater.* 2016, *107*, 484–507. doi:10.1016/j.actamat.2015.05.050
100. Gavras, A. G.; Spangenberger, A. G.; Lados, D. A. Fatigue Crack Growth Microstructural Mechanisms and Texture-Sensitive Predictive Modeling of Lightweight Structural Metals. *Int. J. Fatigue* 2021, *149*, 106278. doi:10.1016/j.ijfatigue.2021.106278
101. Beretta, S.; Lo Conte, A.; Rudlin, J.; Panggabean, D. From Atmospheric Corrosive Attack to Crack Propagation for A1N Railway Axles Steel under Fatigue: Damage Process and Detection. *Eng. Fail. Anal.* 2015, *47*, 252–264. doi:10.1016/j.engfailanal.2014.07.026
102. Beretta, S.; Sangalli, F.; Syeda, J.; Panggabean, D.; Rudlin, J. RAAI Project: Life-Prediction and Prognostics for Railway Axles under Corrosion-Fatigue Damage. *Proc. Struct. Integr.* 2017, *4*, 64–70. doi:10.1016/j.prostr.2017.07.010
103. Gangloff, R. P. Environmental Cracking - Corrosion Fatigue. In *Corrosion Tests and Standards: Application and Interpretation*; Baboian, B., Ed. ASTM International, West Conshohocken, USA, 2005; 302–321.
104. Hoddinott, D. S. Railway Axle Failure Investigations and Fatigue Crack Growth Monitoring of an Axle. *Proc. Inst. Mech. Eng. Part F J. Rail Rapid Transit.* 2004, *218*, 283–292. doi:10.1243/0954409043125897
105. Vermilyea, D. A. A Theory for the Propagation of Stress Corrosion Cracks in Metals. *J. Electrochem. Soc.* 1972, *119*, 405. doi:10.1149/1.2404217
106. Jones, D. A. A Unified Mechanism of Stress Corrosion and Corrosion Fatigue Cracking. *Metall. Trans. A* 1985, *2*, 1133–1141.
107. Transportation Safety Board of Canada. *Railway Investigation Report R01Q0010*. Main Track Derailment, Canadian National Train No. G-894-31-14, Mile 12.56, Drummondville Subdivision, Trudel, Quebec, 2001; pp 1–9.
108. Transportation Safety Board of Canada. *Railway Investigation Report R07T0240*, Main Track Train Derailment Canadian Pacific Railway Freight Train No. 230-25 Mile 42. 80, Belleville Subdivision Tichborne, Ontario. 2007; pp 1–12.
109. Swiss Bureau for Railway Funicular and Boat Accidents. *Schlussbericht der Unfalluntersuchungsstelle Bahnen und Schiffe über die vom in Zugsentgleisung.* Reg. No. 06072601, 2006; pp 1–10. (In German). http://www.sust.admin.ch/pdfs/BS/pdf/4020499.pdf.
110. Australian Transport Safety Bureau. *Derailment of XPT Passenger Train ST22*; Harden, New South Wales. 2006.
111. Schulte-Werning, B.; Beier, M.; Degen, K. G.; Stiebel, D. Research on Noise and Vibration Reduction at DB to Improve the Environmental Friendliness of Railway Traffic. *J. Sound Vib.* 2006, *293*, 1058–1069. doi:10.1016/j.jsv.2005.08.065
112. Giannella, V.; Sepe, R.; Borrelli, A.; De Michele, G.; Armentani, E. Numerical Investigation on the Fracture Failure of a Railway Axle. *Eng. Fail. Anal.* 2021, *129*, 105680. doi:10.1016/j.engfailanal.2021.105680
113. Ishihara, S.; Saka, S.; Nan, Z. Y.; Goshima, T.; Sunada, S. Prediction of Corrosion Fatigue Lives of Aluminium Alloy on the Basis of Corrosion Pit Growth Law. *Fatigue Frac. Eng. Mat. Struct.* 2006, *29*, 472–480. doi:10.1111/j.1460-2695.2006.01018.x
114. Li, H.; Zhang, J.; Wu, S.; Zhang, H.; Fu, Y. Corrosion Fatigue Mechanism and Life Prediction of Railway Axle EA4T Steel Exposed to Artificial Rainwater. *Eng. Fail. Anal.* 2022, *138*, 106319.). doi:10.1016/j.engfailanal.2022.106319
115. Murakami, Y.; Endo, M. The Reality of the Concept of Fatigue Damage in Multiple Step Amplitude Loadings: Reason for Unsuccessful Results of Existing Damage Counting Models. *Int. J. Fatigue* 2022, *154*, 106529. doi:10.1016/j.ijfatigue.2021.106529
116. Hobson, P. D. *The Growth of Short Fatigue Cracks in a Medium Carbon Steel*. PhD Thesis, Department of Mechanical Engineering, University of Sheffield, Sheffield, UK, 1985.
117. Tilly, G. Fatigue of Land-Based Structures. *Int. J. Fatigue* 1985, *7*, 67–78. doi:10.1016/0142-1123(85)90036-2
118. Hurricks, P. L. The Mechanism of Fretting — A Review. *Wear* 1970, *15*, 389–409. doi:10.1016/0043-1648(70)90235-8
119. Horger, O. J. Fatigue of Large Shafts by Fretting Corrosion. In *Proceedings of the International*

Conference on the Fatigue of Metals, Institute of Mechanical Engineers; 1956; p 352.
120. Waterhouse, R. B.; Taylor, D. E. Fretting Debris and the Delamination Theory of Wear. *Wear* 1974, *29*, 337–344. doi:10.1016/0043-1648(74)90019-2
121. Waterhouse, R. B. Fretting Wear. *Wear* 1984, *100*, 107–118. doi:10.1016/0043-1648(84)90008-5
122. Jin, O.; Mall, S. Effects of Slip on Fretting Behavior: Experiments and Analyses. *Wear* 2004, *256*, 671–684. doi:10.1016/S0043-1648(03)00510-6
123. Endo, H.; Marui, E. Studies on Fretting Wear: Influence of Rubbing Surface Materials and Some Considerations. *Wear* 2002, *253*, 795–802. doi:10.1016/S0043-1648(02)00226-0
124. Peng, J. F.; Zhu, M. H.; Cai, Z. B.; Liu, J. H.; Zuo, K. C.; Song, C.; Wang, W. J. On the Damage Mechanisms of Bending Fretting Fatigue. *Tribol. Int.* 2014, *76*, 133–141. doi:10.1016/j.triboint.2013.12.018
125. Fouvry, S.; Kubiak, K. Development of a Fretting-Fatigue Mapping Concept: The Effect of Material Properties and Surface Treatments. *Wear* 2009, *267*, 2186–2199. doi:10.1016/j.wear.2009.09.012
126. Varfolomeev, I.; Luke, M.; Burdack, M. Effect of Specimen Geometry on Fatigue Crack Growth Rates for the Railway Axle Material EA4T. *Eng. Fract. Mech.* 2011, *78*, 742–753. doi:10.1016/j.engfracmech.2010.11.011
127. Foletti, S.; Beretta, S.; Gurer, G. Defect Acceptability under Full-Scale Fretting Fatigue Tests for Railway Axles. *Int. J. Fatigue* 2016, *86*, 34–43. doi:10.1016/j.ijfatigue.2015.08.023
128. Hills, D. A. Mechanics of Fretting Fatigue. *Wear* 1994, *175*, 107–113. doi:10.1016/0043-1648(94)90173-2
129. Varenberg, M.; Halperin, G.; Etsion, I. Different Aspects of the Role of Wear Debris in Fretting Wear. *Wear* 2002, *252*, 902–910. doi:10.1016/S0043-1648(02)00044-3
130. Zheng, J. F.; Luo, J.; Mo, J. L.; Peng, J. F.; Jin, X. S.; Zhu, M. H. Fretting Wear Behaviors of a Railway Axle Steel. *Tribol. Int.* 2010, *43*, 906–911. doi:10.1016/j.triboint.2009.12.031
131. Neu, R. W. Progress in Standardization of Fretting Fatigue Terminology and Testing. *Tribol. Int.* 2011, *44*, 1371–1377. doi:10.1016/j.triboint.2010.12.001
132. Chowdhury, M. A.; Kowser, M. A.; Zobaer Shah, Q. M.; Das, S. Characteristics and Damage Mechanisms of Bending Fretting Fatigue of Materials. *Int. J. Damage Mech.* 2018, *27*, 453–487. doi:10.1177/1056789517693412
133. Lemaitre, J. A Continuous Damage Mechanics Model for Ductile Fracture. *J. Eng. Mater. Technol. Trans. ASME* 1985, *107*, 83–89. doi:10.1115/1.3225775
134. Bhattacharya, B.; Ellingwood, B. Continuum Damage Mechanics Analysis of Fatigue Crack Initiation. *Int. J. Fatigue* 1998, *20*, 631–639. doi:10.1016/S0142-1123(98)00032-2
135. Chaboche, J. L.; Lesne, P. M. a Non-Linear Continuous Fatigue Damage Model. *Fat. Frac. Eng. Mat. Struct.* 1988, *11*, 1–17. doi:10.1111/j.1460-2695.1988.tb01216.x
136. Hojjati-Talemi, R.; Wahab, M. A. Fretting Fatigue Crack Initiation Lifetime Predictor Tool: Using Damage Mechanics Approach. *Tribol. Int.* 2013, *60*, 176–186. doi:10.1016/j.triboint.2012.10.028
137. Hojjati-Talemi, R.; Wahab, M. A.; Giner, E.; Sabsabi, M. Numerical Estimation of Fretting Fatigue Lifetime Using Damage and Fracture Mechanics. *Tribol. Lett.* 2013, *52*, 11–25. doi:10.1007/s11249-013-0189-8
138. Quraishi, S. M.; Khonsari, M. M.; Baek, D. K. A Thermodynamic Approach for Predicting Fretting Fatigue Life. *Tribol. Lett.* 2005, *19*, 169–175. doi:10.1007/s11249-005-6143-7
139. Chaudonneret, M. A Simple and Efficient Multiaxial Fatigue Damage Model for Engineering Applications of Macro-Crack Initiation. *J. Eng. Mater. Technol. Trans. ASME* 1993, *115*, 373–379. doi:10.1115/1.2904232
140. Crossland, B. Effect of Large Hydrostatic Pressures on the Torsional Fatigue Strength of an Alloy Steel. *Proc. Int. Fatigue Met.* 1956, *138*, 138–149.
141. Findley, W. N. A Theory for the Effect of Mean Stress on Fatigue of Metals under Combined Torsion and Axial Load or Bending. *J. Eng. Ind.* 1959, *81*, 301–305. doi:10.1115/1.4008327
142. McDiarmid, D. L. A General Criterion for High Cycle Multiaxial Fatigue Failure. *Fatigue Frac. Eng. Mat. Struct.* 1991, *14*, 429–453. doi:10.1111/j.1460-2695.1991.tb00673.x
143. Lykins, C. D.; Mall, S.; Jain, V. A Shear Stress-Based Parameter for Fretting Fatigue Crack Initiation. *Fatigue Fract. Eng. Mater. Struct.* 2001, *24*, 461–473. doi:10.1046/j.1460-2695.2001.00412.x
144. Fatemi, A.; Socie, D. F. A Critical Plane Approach to Multiaxial Fatigue Damage Including out-of-Phase Loading. *Fatigue Frac. Eng. Mat. Struct.* 1988, *11*, 149–165. doi:10.1111/j.1460-2695.1988.tb01169.x
145. Szolwinski, M. P.; Farris, T. N. Mechanics of Fretting Fatigue Crack Formation. *Wear* 1996, *198*, 93–107. doi:10.1016/0043-1648(96)06937-2
146. Liu, K. C. A Method Based on Virtual Strain-Energy Parameters for Multiaxial Fatigue Life Prediction. *ASTM Spec. Tech. Publ.* 1993, *1191*, 67–67.
147. Brown, M. W.; Miller, K. J. A Theory for Fatigue Failure under Multiaxial Stress-Strain Conditions. *Proc. Inst. Mech. Eng.* 1973, *187*, 745–755. doi:10.1243/PIME_PROC_1973_187_161_02
148. Ding, J.; Houghton, D.; Williams, E. J.; Leen, S. B. Simple Parameters to Predict Effect of Surface Damage on Fretting Fatigue. *Int. J. Fatigue* 2011, *33*, 332–342. doi:10.1016/j.ijfatigue.2010.09.008
149. Ruiz, C.; Boddington, P. H. B.; Chen, K. C. An Investigation of Fatigue and Fretting in a Dovetail Joint. *Exp. Mech.* 1984, *24*, 208–217. doi:10.1007/BF02323167
150. Wharton, M. H.; Waterhouse, R. B.; Hirakawa, K.; Nishioka, K. The Effect of Different Contact Materials on the Fretting Fatigue Strength of an Aluminium Alloy. *Wear* 1973, *26*, 253–260. doi:10.1016/0043-1648(73)90139-7

151. Bhatti, N. A.; Abdel Wahab, M. Fretting Fatigue Crack Nucleation: A Review. *Tribol. Int.* 2018, *121*, 121–138. doi:10.1016/j.triboint.2018.01.029
152. Coffin, L. F. A Study of the Effect of Cyclic Thermal Stresses on Ductile Metal. *Trans. Am. Soc. Mech. Eng.* 1954, *76*, 931–949. doi:10.1115/1.4015020
153. Gelfi, M.; La Vecchia, G. M.; Lecis, N.; Troglio, S. Relationship between through-Thickness Residual Stress of CrN-PVD Coatings and Fatigue Nucleation Sites. *Surf. Coatings Technol.* 2005, *192*, 263–268. doi:10.1016/j.surfcoat.2004.05.032
154. Niederhauser, S.; Karlsson, B. Fatigue Behaviour of Co–Cr Laser Cladded Steel Plates for Railway Applications. *Wear* 2005, *258*, 1156–1164. doi:10.1016/j.wear.2004.03.026
155. Korzynski, M.; Pacana, A.; Cwanek, J. Fatigue Strength of Chromium Coated Elements and Possibility of Its Improvement with Slide Diamond Burnishing. *Surf. Coatings Technol.* 2009, *203*, 1670–1676. doi:10.1016/j.surfcoat.2008.12.022
156. Ibrahim, A.; Berndt, C. C. Fatigue and Deformation of HVOF Sprayed WC–Co Coatings and Hard Chrome Plating. *Mater. Sci. Eng. A* 2007, *456*, 114–119. doi:10.1016/j.msea.2006.12.030
157. Klenam, D. E. P. Composition Refinement of Medium Carbon-Low Alloy Steels to Improve Wear and Corrosion Resistance for Rail Axle Applications; PhD Thesis, School of Chemical and Metallurgical Engineering, University of the Witwatersrand, Johannesburg, South Africa, 2019.
158. Pickering, F. B. *Physical Metallurgy and the Design of Steels*; Applied Science Publishers, London, UK, 1978.
159. Bhadeshia, H. K. D. H. The Lower Bainite Transformation and the Significance of Carbide Precipitation. *Acta Metall.* 1980, *28*, 1103–1114. doi:10.1016/0001-6160(80)90093-0
160. Cantini, S.; Ghidini, A. *A Basic Life Estimates for Railway Axle Materials under Constant Amplitude Loading and LEFM Hypothesis*; Lucchini Internal Report R&D R015-2003, Italy, 2003.
161. Zhou, J.; et al. The Comprehensive Effect of Controlled Cooling and Si/Mn Elements on the Structure-Property Relationship of a Novel Wire Rod. *J. Mater. Eng. Perform.* 2022, 1–9.
162. Beretta, S.; Zerbst, U. Damage Tolerance of Railway Axles. *Eng. Fract. Mech.* 2011, *78*, 713. doi:10.1016/j.engfracmech.2011.02.014
163. Pokorný, P.; Náhlík, L.; Hutař, P. Influence of Threshold Values on Residual Fatigue Lifetime of Railway Axles under Variable Amplitude Loading. *Proc. Eng.* 2015, *101*, 380–385. doi:10.1016/j.proeng.2015.02.046
164. Moon, A.; Sangal, S.; Mondal, K. Corrosion Behaviour of New Railway Axle Steels. *Trans. Indian Inst. Met.* 2013, *66*, 33–41. doi:10.1007/s12666-012-0167-0
165. Association of American Railroads. Manual of Standards and Recommended Practice, Section G, Part 1, Washington DC, USA, 1990.
166. Mancini, G.; Corbizi, A.; Lombardo, F.; Cervello, S. Design of Railway Axle in Compliance with the European Norms: High Strength Alloyed Steels Compared to Standard Steels. In *Proceedings of World Congress on Railway Research*; 2006, pp 1–12.
167. Zhang, J. W. W.; Lu, L. T. T.; Shiozawa, K.; Zhou, W. N. N.; Zhang, W. H. H. Effect of Nitrocarburizing and Post-Oxidation on Fatigue Behavior of 35CrMo Alloy Steel in Very High Cycle Fatigue Regime. *Int. J. Fatigue* 2011, *33*, 880–886. doi:10.1016/j.ijfatigue.2011.01.016
168. Zhang, J.; Lu, L.; Cui, G.; Shen, X.; Yi, H.; Zhang, W. Effect of Process Temperature on the Microstructure and Properties of Gas Oxynitrocarburized 35CrMo Alloy Steel. *Mater. Des.* 2010, *31*, 2654–2658. doi:10.1016/j.matdes.2009.11.068
169. Yang, B.; Zhao, Y. Experimental Research on Dominant Effective Short Fatigue Crack Behavior for Railway LZ50 Axle Steel. *Int. J. Fatigue* 2012, *35*, 71–78. doi:10.1016/j.ijfatigue.2010.11.012
170. Beretta, S.; Carboni, M.; Cantini, S.; Ghidini, A. Application of Fatigue Crack Growth Algorithms to Railway Axles and Comparison of Two Steel Grades. *Proc. Inst. Mech. Eng. Part F J. Rail Rapid Transit.* 2004, *218*, 317–326. doi:10.1243/0954409043125888
171. Beretta, S.; Carboni, M. Variable Amplitude Fatigue Crack Growth in a Mild Steel for Railway Axles: Experiments and Predictive Models. *Eng. Fract. Mech.* 2011, *78*, 848–862. doi:10.1016/j.engfracmech.2010.11.019
172. Beretta, S.; Carboni, M.; Cervello, S. Design Review of a Freight Railway Axle: Fatigue Damage versus Damage Tolerance. *Materialwissenschaft und Werkstofftechnik* 2011, *42*, 1099–1104. doi:10.1002/mawe.201100916
173. UN16787-71. Assi fucinati di acciano special legato, bonificati, ad elevate caratterístieche di fatica a di tenacita per sale monatete di rotabili ferroviari. Qualita: Preserizoni e Prove, 1971.
174. Vickerman, R. High-Speed Rail in Europe: Experience and Issues for Future Development. *Ann. Reg. Sci.* 1997, *31*, 21–38. doi:10.1007/s001680050037
175. Zhang, J. W.; Lu, L. T.; Wu, P. B.; Ma, J. J.; Wang, G. G.; Zhang, W. H. Inclusion Size Evaluation and Fatigue Strength Analysis of 35CrMo Alloy Railway Axle Steel. *Mater. Sci. Eng. A* 2013, *562*, 211–217. doi:10.1016/j.msea.2012.11.035
176. Abbasi, E.; Luo, Q.; Owens, D. A Comparison of Microstructure and Mechanical Properties of Low-Alloy-Medium-Carbon Steels after Quench-Hardening. *Mater. Sci. Eng. A* 2018, *725*, 65–75. doi:10.1016/j.msea.2018.04.012
177. Rackwitz, J.; Yu, Q.; Yang, Y.; Laplanche, G.; George, E. P.; Minor, A. M.; Ritchie, R. O. Effects of Cryogenic Temperature and Grain Size on Fatigue-Crack Propagation in the Medium-Entropy CrCoNi Alloy. *Acta Mater.* 2020, *200*, 351–365. doi:10.1016/j.actamat.2020.09.021
178. Jo, Y. H.; Doh, K.-Y.; Kim, D. G.; Lee, K.; Kim, D. W.; Sung, H.; Sohn, S. S.; Lee, D.; Kim, H. S.; Lee, B.-J.; et al. Cryogenic-Temperature Fracture Toughness Analysis of Non-Equi-Atomic V10Cr10Fe45Co20Ni15 High-Entropy Alloy. *J.*

Alloys Compd. 2019, *809*, 151864. doi:10.1016/j.jallcom.2019.151864
179. Japanese Standards. *Japanese Industrial Standards JIS E 4502-1-2001 Axles for Railway Rolling Stock - Quality Requirements*, Japan, 2001.
180. Japanese Standards. *Japanese Industrial Standards JIS E 4502-2-2001 Axles for Railway Rolling Stock - Dimensional Requirements*, Japan, 2001.
181. Gao, J.; et al. Influence of Artificial Defects on Fatigue Strength of Induction Hardened S38C Axles. *Int. J. Fatigue* 2020, *139*, 105746.
182. Horger, O. Wheel, axle and rail stress Problem Related to Higher Capacity Cars-Axle Problems. In *Anthology of Rail Vehicle Dynamics 3, Axles, Wheels and Rail-Wheel Interaction*; American Society of Mechanical Engineers, 1973, pp 49–58.
183. ASTM Standard A 730-93. *Standard Specification for Forgings, Carbon and Alloy Steels for Railway Use*, ASTM International, Material Park, OH, USA, 1993.
184. Zhu, Y.; Kang, G.; Ding, J.; Zhu, M. Study on Bending Fretting Fatigue of LZ50 Axle Steel considering Ratchetting by Finite Element Method. *Fatigue Fract. Eng. Mater. Struct.* 2013, *36*, 127–138. doi:10.1111/j.1460-2695.2012.01705.x
185. Japanese Standards. *Japan Association of Rolling Stock Industries Standards JRIS J 0401-2007 Rolling Stock - Induction-Hardened Axles for High Speed Vehicle*, 2007.
186. Pokorný, P.; et al. Influence of Heat Treatment-Induced Residual Stress on Residual Fatigue Life of Railway Axles. *Theor. Appl. Fract. Mech.* 2020, *109*, 102732.
187. Itagaki, M.; Nozue, R.; Watanabe, K.; Katayama, H.; Noda, K. Electrochemical Impedance of Thin Rust Film of Low-Alloy Steels. *Corros. Sci.* 2004, *46*, 1301–1310. doi:10.1016/j.corsci.2003.08.002
188. Wranglén, G. Review Article on the Influence of Sulphide Inclusions on the Corrodibility of Fe and Steel. *Corros. Sci.* 1969, *9*, 585–602. doi:10.1016/S0010-938X(69)80114-9
189. Wranglen, G. Pitting and Sulphide Inclusions in Steel. *Corros. Sci.* 1974, *14*, 331–349. doi:10.1016/S0010-938X(74)80047-8
190. Moon, A. P.; Sangal, S.; Layek, S.; Giribaskar, S.; Mondal, K. Corrosion Behavior of High-Strength Bainitic Rail Steels. *Metall. Mater. Trans. A* 2015, *46*, 1500–1518. doi:10.1007/s11661-014-2732-0
191. Guo, J.; Yang, S.; Shang, C.; Wang, Y.; He, X. Influence of Carbon Content and Microstructure on Corrosion Behaviour of Low Alloy Steels in a Cl-Containing Environment. *Corros. Sci.* 2009, *51*, 242–251. doi:10.1016/j.corsci.2008.10.025
192. Liang, C.; Yu, M.; Ma, H.; Chen, H. Effect of Vacuum Hot Pressing on Plasma-Sprayed Molybdenum Coatings on Rail Vehicle Axle Steel. *J. Therm. Spray Technol.* 2019, *28*, 893–903. doi:10.1007/s11666-019-00862-4
193. Miracle, D.; Majumdar, B.; Wertz, K.; Gorsse, S. New Strategies and Tests to Accelerate Discovery and Development of Multi-Principal Element Structural Alloys. *Scr. Mater.* 2017, *127*, 195–200. doi:10.1016/j.scriptamat.2016.08.001
194. Liao, Z.; Yang, B.; Dai, S.; Xiao, S.; Yang, G.; Zhu, T. Effects of Stress Amplitude Ratio and Phase Angle on Short Fatigue Crack Behavior and Fracture Mode of EA4T Steel. *J. Mater. Eng. Perform.* 2021, *30*, 2853–2863. doi:10.1007/s11665-021-05607-5
195. Ritchie, R. O. The Conflicts between Strength and Toughness. *Nat. Mater.* 2011, *10*, 817–822. doi:10.1038/nmat3115
196. Mistry, P. J.; Johnson, M. S. Lightweighting of Railway Axles for the Reduction of Unsprung Mass and Track Access Charges. *Proc. Inst. Mech. Eng. Part F J. Rail Rapid Transit.* 2020, *234*, 958–968. doi:10.1177/0954409719877774
197. Klenam, D. E. P.; Rahbar, N.; Soboyejo, W. O. Mechanical Properties of Complex Concentrated Alloys: Implications for Structural Integrity. In *Reference Module in Materials Science and Materials Engineering*; Elsevier, Philadelphia, USA, 2022. doi:10.1016/B978-0-12-822944-6.00047-5
198. Klenam, D. E. P.; Rahbar, N.; Soboyejo, W. O. Critical Review of Factors Hindering Scalability of Complex Concentrated Alloys. In *Reference Module in Materials Science and Materials Engineering*; Elsevier, Philadelphia, USA, 2022. doi:10.1016/B978-0-12-822944-6.00051-7
199. Klenam, D. E. P.; et al. Complex Concentrated Alloys: A Cornucopia of Possible Structural and Functional Applications. In *Reference Module in Materials Science and Materials Engineering*; Elsevier, Philadelphia, USA, 2022. doi:10.1016/B978-0-12-822944-6.00056-6
200. Fintová, S.; Pokorný, P.; Fajkoš, R.; Hutař, P. EA4T Railway Axle Steel Fatigue Behavior under Very High-Frequency Fatigue Loading. *Eng. Fail. Anal.* 2020, *115*, 104668. doi:10.1016/j.engfailanal.2020.104668
201. Yang, J. P.; Zhao, Y. X.; Wang, J. G. Appropriate Method for Railway Vehicle Axle Journal Bearing Capacity Evaluation. In *2020 7th International Forum on Electrical Engineering and Automation (IFEEA)*, 2020, pp 1010–1016.
202. Luo, Y.; Wu, S.; Zhao, X.; Hu, Y.; Li, C.; Shen, Z.; Zhong, X. Three-Dimensional Correlation of Damage Criticality with the Defect Size and Lifetime of Externally Impacted 25CrMo4 Steel. *Mater. Des.* 2020, *195*, 109001. doi:10.1016/j.matdes.2020.109001
203. Pourheidar, A.; Regazzi, D.; Cervello, S.; Foletti, S.; Beretta, S. Fretting Fatigue Analysis of Full-Scale Railway Axles in Presence of Artificial Micro-Notches. *Tribol. Int.* 2020, *150*, 106383. doi:10.1016/j.triboint.2020.106383
204. He, J.; Cui, Y.; Liu, Y.; Wang, H. Probabilistic Analysis of Crack Growth in Railway Axles Using a Gaussian Process. *Adv. Mech. Eng.* 2020, *12*, 1–12.
205. Rana, R. Low-Density Steels. *Jom* 2014, *66*, 1730–1733. doi:10.1007/s11837-014-1137-2
206. Zuazo, I.; Hallstedt, B.; Lindahl, B.; Selleby, M.; Soler, M.; Etienne, A.; Perlade, A.; Hasenpouth, D.; Massardier-Jourdan, V.; Cazottes, S.; et al. Low-Density Steels: Complex Metallurgy for Automotive Applications. *J. Mater.* 2014, *66*, 1747–1758. doi:10.1007/s11837-014-1084-y

207. Chen, S.; Rana, R.; Haldar, A.; Ray, R. K. Current State of Fe-Mn-Al-C Low Density Steels. *Prog. Mater. Sci.* 2017, *89*, 345–391. doi:10.1016/j.pmatsci.2017.05.002
208. Klenam, D.; Rahbar, N.; Soboyejo, W. Critical Review of Limitations of Equiatomic Composition Alloying Strategy of Complex Concentrated Alloys. In *Reference Module in Materials Science and Materials Engineering*; Elsevier, Philadelphia, USA, 2022. doi:10.1016/B978-0-12-822944-6.00055-4
209. Gludovatz, B.; et al. Exceptional Damage-Tolerance of a Medium Entropy Alloy CrCoNi at Cryogenic Temperatures. *Nat. Commun.* 2016, *7*, 1–8.
210. Xue, P.; et al. CrCoNi Medium-Entropy Alloy Thin-Walled Parts Manufactured by Laser Metal Deposition: Microstructure Evolution and Mechanical Anisotropy. *Mater. Sci. Eng. A* 2021, *817*, 104743.
211. Zheng, X.; Xie, W.; Zeng, L.; Wei, H.; Zhang, X.; Wang, H. Achieving High Strength and Ductility in a Heterogeneous-Grain-Structured CrCoNi Alloy Processed by Cryorolling and Subsequent Short-Annealing. *Mater. Sci. Eng. A* 2021, *821*, 141610. doi:10.1016/j.msea.2021.141610
212. Li, Z.; Pradeep, K. G.; Deng, Y.; Raabe, D.; Tasan, C. C. Metastable High-Entropy Dual-Phase Alloys Overcome the Strength-Ductility Trade-off. *Nature* 2016, *534*, 227–230. doi:10.1038/nature17981
213. Dong, Y.; Duan, S.; Huang, X.; Li, C.; Zhang, Z. Excellent Strength-Ductility Synergy in as-Cast Al0.6CoCrFeNi2Mo0.08V0.04 High-Entropy Alloy at Room and Cryogenic Temperatures. *Mater. Lett.* 2021, *294*, 129778. doi:10.1016/j.matlet.2021.129778
214. Yi, J.; Wang, L.; Zeng, L.; Xu, M.; Yang, L.; Tang, S. Excellent Strength-Ductility Synergy in a Novel Single-Phase Equiatomic CoFeNiTiV High Entropy Alloy. *Int. J. Refract. Met. Hard Mater.* 2021, *95*, 105416. doi:10.1016/j.ijrmhm.2020.105416
215. Zhang, W.; Ma, Z.; Zhao, H.; Ren, L. Breakthrough the Strength-Ductility Trade-off in a High-Entropy Alloy at Room Temperature via Cold Rolling and Annealing. *Mater. Sci. Eng. A* 2021, *800*, 140264. doi:10.1016/j.msea.2020.140264
216. Liu, Y.; He, Y.; Cai, S. Effect of Gradient Microstructure on the Strength and Ductility of Medium-Entropy Alloy Processed by Severe Torsion Deformation. *Mater. Sci. Eng. A* 2021, *801*, 140429. doi:10.1016/j.msea.2020.140429
217. Jiang, K.; Gan, B.; Li, J.; Dou, Q.; Suo, T. Towards Strength-Ductility Synergy in a CrCoNi Solid Solution Alloy via Nanotwins. *Mater. Sci. Eng. A* 2021, *816*, 141298. doi:10.1016/j.msea.2021.141298
218. Zhang, D. D.; Wang, H.; Zhang, J. Y.; Xue, H.; Liu, G.; Sun, J. Achieving Excellent Strength-Ductility Synergy in Twinned NiCoCr Medium-Entropy Alloy via Al/Ta co-Doping. *J. Mater. Sci. Technol.* 2021, *87*, 184–195. doi:10.1016/j.jmst.2021.01.060
219. Li, G.; Liu, M.; Lyu, S.; Nakatani, M.; Zheng, R.; Ma, C.; Li, Q.; Ameyama, K. Simultaneously Enhanced Strength and Strain Hardening Capacity in FeMnCoCr High-Entropy Alloy via Harmonic Structure Design. *Scr. Mater.* 2021, *191*, 196–201. doi:10.1016/j.scriptamat.2020.09.036
220. Huang, L.; et al. Simultaneously Enhanced Strength-Ductility of AlCoCrFeNi 2.1 Eutectic High-Entropy Alloy via Additive Manufacturing. Mater. Sci. Eng. A, 2022, *830*, 142327
221. Reddy, S. R.; Yoshida, S.; Bhattacharjee, T.; Sake, N.; Lozinko, A.; Guo, S.; Bhattacharjee, P. P.; Tsuji, N. Nanostructuring with Structural-Compositional Dual Heterogeneities Enhances Strength-Ductility Synergy in Eutectic High Entropy Alloy. *Sci. Rep.* 2019, *9*, 1–10. doi:10.1038/s41598-019-47983-y
222. Sun, S.; Gao, P.; Sun, G.; Cai, Z.; Hu, J.; Han, S.; Lian, J.; Liao, X. Nanostructuring as a Route to Achieve Ultra-Strong High- and Medium-Entropy Alloys with High Creep Resistance. *J. Alloys Compd.* 2020, *830*, 154656. doi:10.1016/j.jallcom.2020.154656
223. Koch, C. C. Nanocrystalline High-Entropy Alloys. *J. Mater. Res.* 2017, *32*, 3435–3444. doi:10.1557/jmr.2017.341
224. Sharma, A. S.; Yadav, S.; Biswas, K.; Basu, B. High-Entropy Alloys and Metallic Nanocomposites: Processing Challenges, Microstructure Development and Property Enhancement. *Mater. Sci. Eng. R Rep.* 2018, *131*, 1–42. doi:10.1016/j.mser.2018.04.003
225. Wei, S.; He, F.; Tasan, C. C. Metastability in High-Entropy Alloys: A Review. *J. Mater. Res.* 2018, *33*, 2924–2937. doi:10.1557/jmr.2018.306
226. He, Z. F.; Jia, N.; Ma, D.; Yan, H. L.; Li, Z. M.; Raabe, D. Joint Contribution of Transformation and Twinning to the High Strength-Ductility Combination of a FeMnCoCr High Entropy Alloy at Cryogenic Temperatures. *Mater. Sci. Eng. A* 2019, *759*, 437–447. doi:10.1016/j.msea.2019.05.057
227. Li, J.; Chen, H.; Fang, Q.; Jiang, C.; Liu, Y.; Liaw, P. K. Unraveling the Dislocation-Precipitate Interactions in High-Entropy Alloys. *Int. J. Plast.* 2020, *133*, 102819. doi:10.1016/j.ijplas.2020.102819
228. Soto, A. O.; Salgado, A. S.; Niño, E. B. Thermodynamic Analysis of High Entropy Alloys and Their Mechanical Behavior in High and Low-Temperature Conditions with a Microstructural approach - A Review. *Intermetallics* 2020, *124*, 106850. doi:10.1016/j.intermet.2020.106850
229. Song, H.; Yang, J.; Jo, Y. H.; Song, T.; Kim, H. S.; Lee, B.-J.; Lee, S. Excellent Combination of Cryogenic-Temperature Strength and Ductility of High-Entropy-Alloy-Cored Multi-Layered Sheet. *J. Alloys Compd.* 2019, *797*, 465–470. doi:10.1016/j.jallcom.2019.05.088
230. Xie, J.; Zhang, S.; Sun, Y.; Hao, Y.; An, B.; Li, Q.; Wang, C.-A. Microstructure and Mechanical Properties of High Entropy CrMnFeCoNi Alloy Processed by Electopulsing-Assisted Ultrasonic Surface Rolling. *Mater. Sci. Eng. A* 2020, *795*, 140004. doi:10.1016/j.msea.2020.140004
231. Zhu, Y.; Zhou, S.; Wang, L.; Liang, Y.-J.; Xue, Y.; Wang, L. Improving the Ductility of High-Strength Multiphase NiAl Alloys by Introducing Multiscale High-Entropy Phases and Martensitic Transformation. *Mater. Sci. Eng. A* 2021, *808*, 140949. doi:10.1016/j.msea.2021.140949
232. An, Z.; Mao, S.; Liu, Y.; Zhou, H.; Zhai, Y.; Tian, Z.; Liu, C.; Zhang, Z.; Han, X. Hierarchical Grain Size

and Nanotwin Gradient Microstructure for Improved Mechanical Properties of a Non-Equiatomic CoCrFeMnNi High-Entropy Alloy. *J. Mater. Sci. Technol.* 2021, *92*, 195–207. doi:10.1016/j.jmst.2021.02.059

233. Hu, Y.; Dong, Y.; Huang, X.; Li, C.; Zhang, Z. Microstructure Characteristics of a High-Entropy-Alloy Intermetallic Laminate Composite. *Mater. Lett.* 2020, *273*, 127937. doi:10.1016/j.matlet.2020.127937
234. Li, Z.; Raabe, D. Strong and Ductile Non-Equiatomic High-Entropy Alloys: Design, Processing, Microstructure, and Mechanical Properties. *Jom (1989)* 2017, *69*, 2099–2106. doi:10.1007/s11837-017-2540-2
235. Li, J.; Huang, Y.; Meng, X.; Xie, Y. A Review on High Entropy Alloys Coatings: Fabrication Processes and Property Assessment. *Adv. Eng. Mater.* 2019, *1900343*, 1–27.
236. Bagherifard, S.; Guagliano, M. Fatigue Performance of Cold Spray Deposits: Coating, Repair and Additive Manufacturing Cases. *Int. J. Fatigue* 2020, *139*, 105744. doi:10.1016/j.ijfatigue.2020.105744
237. Srikanth, A.; Mohammed Thalib Basha, G.; Venkateshwarlu, B. A Brief Review on Cold Spray Coating Process. *Mater. Today Proc.* 2020, *22*, 1390–1397. doi:10.1016/j.matpr.2020.01.482
238. Yin, S.; Cavaliere, P.; Aldwell, B.; Jenkins, R.; Liao, H.; Li, W.; Lupoi, R. Cold Spray Additive Manufacturing and Repair: Fundamentals and Applications. *Addit. Manuf.* 2018, *21*, 628–650. doi:10.1016/j.addma.2018.04.017
239. Assadi, H.; Kreye, H.; Gärtner, F.; Klassen, T. Cold Spraying – A Materials Perspective. *Acta Mater.* 2016, *116*, 382–407. doi:10.1016/j.actamat.2016.06.034
240. Blose, R. E.; Walker, B. H.; Walker, R. M.; Froes, S. H. New Opportunities to Use Cold Spray Process for Applying Additive Features to Titanium Alloys. *Met. Powder Rep.* 2006, *61*, 30–37. doi:10.1016/S0026-0657(06)70713-5
241. Li, W.; Cao, C.; Yin, S. Solid-State Cold Spraying of Ti and Its Alloys: A Literature Review. *Prog. Mater. Sci.* 2020, *110*, 100633. doi:10.1016/j.pmatsci.2019.100633
242. Zhang, Z.; Liu, F.; Han, E. H.; Xu, L. Mechanical and Corrosion Properties in 3.5% NaCl Solution of Cold Sprayed Al-Based Coatings. *Surf. Coatings Technol.* 2020, *385*, 125372. doi:10.1016/j.surfcoat.2020.125372
243. Chen, C.; Xie, Y.; Yan, X.; Ahmed, M.; Lupoi, R.; Wang, J.; Ren, Z.; Liao, H.; Yin, S. Tribological Properties of Al/Diamond Composites Produced by Cold Spray Additive Manufacturing. *Addit. Manuf.* 2020, *36*, 101434. doi:10.1016/j.addma.2020.101434
244. Cantor, B.; Chang, I. T. H.; Knight, P.; Vincent, A. J. B. Microstructural Development in Equiatomic Multicomponent Alloys. *Mater. Sci. Eng. A* 2004, *375–377*, 213–218. doi:10.1016/j.msea.2003.10.257
245. Manzoni, A. M.; Glatzel, U. New Multiphase Compositionally Complex Alloys Driven by the High Entropy Alloy Approach. *Mater. Charact.* 2019, *147*, 512–532. doi:10.1016/j.matchar.2018.06.036